STRUCTURE AND KINEMATICS OF THE SUZUME FAULT, OKITSU MELANGE, SHIMANTO ACCRETIONARY COMPLEX, JAPAN

A Thesis

by

TAKAMASA KANAYA

Submitted to the Office of Graduate Studies of
Texas A&M University
in partial fulfillment of the requirements for the degree of

MASTER OF SCIENCE

December 2006

Major Subject: Geology

STRUCTURE AND KINEMATICS OF THE SUZUME FAULT, OKITSU MELANGE, SHIMANTO ACCRETIONARY COMPLEX, JAPAN

A Thesis

by

TAKAMASA KANAYA

Submitted to the Office of Graduate Studies of
Texas A&M University
in partial fulfillment of the requirements for the degree of

MASTER OF SCIENCE

Approved by:

Chair of Committee,	Frederick M. Chester
Committee Members,	Judith S. Chester
	Adam Klaus
Head of Department,	Richard L. Carlson

December 2006

Major Subject: Geology

ABSTRACT

Structure and Kinematics of the Suzume Fault, Okitsu Mélange,
Shimanto Accretionary Complex, Japan. (December 2006)
Takamasa Kanaya, B.S., Kochi University
Chair of Advisory Committee: Dr. Frederick M. Chester

The Okitsu mélange in the Shimanto accretionary complex, the onshore extension of the modern Nankai accretionary prism, consists of a kilometer-size duplex of oceanic basalt and trench-fill sedimentary rocks, and is thought to represent rocks underplated to the prism along the subduction plate-boundary at seismogenic depth. An internal, horse-bounding thrust of the duplex, referred to as the Suzume fault, juxtaposes basalt in the hanging wall and sedimentary rocks in the footwall. Structure and fabric of the fault was characterized at the mesoscale to investigate the processes and structural evolution along a plate-boundary décollement. The fault zone in the hanging wall consists of decimeter-thick ultracataclasite bounded by a several m thick zone of fractured basalt, and likely records 2+ km displacement along the thrust. The footwall consists of decimeter-thick ultracataclasite bounded by a 20-m-thick zone of ductile shear in flattened sedimentary host rock, and likely records 30+ km of displacement. The asymmetric structure across the Suzume fault, as well as inferred displacement fields and timing relations, are consistent with a tectonic model in which the footwall records early ductile, compactive deformation of poorly consolidated sediments during underthrusting at the prism toe region, followed by extremely localized cataclasis at the underplating depth. In contrast, the hanging wall is deformed by intense cataclasis, and only during underplating. Deformation style and strain state in the footwall of the Suzume fault is qualitatively similar to the modern Costa Rica underthrust section at the toe region. Similarity in the structure and fabric of the hanging wall between the Suzume fault and modern décollement zones sampled through scientific drilling suggests that intense cataclasis under horizontal contraction likely is a common feature for the hanging wall of the

décollement zone throughout the toe to underplating regions. Structures in the Suzume fault that are not in common with the modern décollements imply progressive consolidation during underthrusting from the toe to underplating depths may be responsible for the localization of shear in the footwall. At several kilometers depth, displacement along the plate boundary is likely accommodated within an extremely narrow zone as recorded in the ultracataclasite of the Suzume fault.

DEDICATION

To Shigenori Okino

Wish you were alive so that I could thank you for your hospitality.

and

To Umeko Okino and Rider's Inn Nakatosa

ACKNOWLEDGMENTS

Foremost, I am extremely grateful to having Dr. Frederick Chester as my advisor and getting to learn his scientific methodology and humble attitude as a scientist. He always tried to share what I should learn most in his knowledge and experience with me. I am so fortunate to have a role model scientist like him in my research career. I also thank him for his patience with my stubbornness.

I express my appreciation to Drs. Judith Chester and Adam Klaus for their constructive criticism and sincere efforts to improve this thesis. I am grateful to Dr. Brann Johnson for his continual, warm encouragement and for showing me how a teacher could influence youth with his enthusiasm. I also thank Drs. Andreas Kronenberg, David Wiltschko, and John Spang for their advice on my research.

I cannot thank my colleague students in the Center for Tectonophysics enough. Daily mentoring by soon-to-be-Drs. Pablo Cervantes and Martin Finn and kindness by Jen Bobich and James Orofino to help me to live in a foreign country are greatly appreciated.

I greatly acknowledge the Department of Geology & Geophysics at TAMU for financial support throughout my degree and providing me an opportunity to be a teaching assistant. Working with students in Geology 101 was one of the best experiences in my life; it has inspired me to pursue a career goal of helping young men and women to develop.

Financial support for this study was provided by Department of Geology & Geophysics at TAMU and a G.S.A. Graduate Research Grant. Polyester resin was donated by Reichold to the Department of Geology & Geophysics at TAMU.

Hospitality and love from Alan and Pat Gillogly, my host parents in College Station, allowed me to have a wonderful study abroad experience. I am extremely grateful to the people I have had friendship with in the Texas A&M Community.

I am indebted to Dr. Arito Sakaguchi, my former advisor, and faculty in the Department of Geology at Kochi University for introducing me to fascinating Mother Nature on Shikoku Island and for sharing with me how joyful being a geologist is.

Special appreciation goes to my former colleagues at Kochi University, especially Dr. Hideki Mukoyoshi, for mutual stimulation and field assistance. I also thank Dr. Yoshitaka Hashimoto for his advice and the Department of Geology at Kochi University for allowing me to use the rock preparation facility while I was in Kochi for my field work.

Finally, for their love, I am so grateful to my parents, Ituro and Yae Kanaya, my brothers, Tomohiro and Ken-ichi Kanaya, and my grandmothers, Hisako Kanaya and Yasue Ohtsuki.

TABLE OF CONTENTS

LIST OF FIGURES

FIGURE Page

1. INTRODUCTION

Plate boundary fault zones have received considerable attention because of the direct relation to earthquakes (e.g. Scholz, 1990; Moore and Saffer, 2001) and effects on the mechanical and hydrological properties of lithosphere (e.g. Screaton et al., 1990; Hickman, 1991). The geometry of large-displacement, brittle fault zones may be regarded as a single slip-surface at the macroscopic scale, but actually consists of a tabular zone often tens to hundreds meter thick (e.g. Wallace and Morris, 1986; Chester and Logan, 1986; Faulkner et al., 2003). Fault zones have been described by a simple model in which the majority of fault displacement is accommodated in a fault core that is bounded by a damage zone of fault related deformation that diminishes in intensity outward into relatively undeformed host rocks (e.g. Chester et al., 1993; Caine et al., 1996). The fault cores, meters in thickness, are often defined by the development of cataclasite and shear fabric, and possibly by the presence of slip surfaces and chemically altered rocks (e.g. Evans and Chester, 1995; Ohtani et al., 2000). The damage zones, tens to hundreds meters in thickness, may consist of secondary fractures, faults, and folds (Bruhn et al., 1994; Shipton and Cowie, 2001; Berg and Skar, 2005). Fault zone models, such as the fault core and damage zone model, are employed in mechanical analysis of faulting processes (e.g. Rice, 1992; Ben-Zion and Sammis, 2003), petrophysical analysis of fault zones (e.g. Evans et al., 1997; Rawling et al., 2001), and geophysical monitoring and imaging of natural fault zones (e.g. Bourlange et al., 2003; Gettemy et al., 2004).

The structure of faults is expected to reflect both extrinsic (e.g. pressure, temperature, loading condition, displacement) and intrinsic (e.g. lithology, porosity) parameters. Because such parameters are strongly tied to a regional tectonics, one might hypothesize that faulting processes and fault zone structure strongly reflect tectonic setting. For example, plate-boundary décollements in subduction zones are expected to differ from many other plate boundary faults because they are characterized by (1) a considerable amount of focused fluid flow and mass transfer due to progressive consolidation and

---

This thesis follows the format of Journal of Structural Geology.

metamorphism during subduction (e.g. Moore and Saffer, 2001), (2) smaller displacements up to a few tens of kilometers (e.g. Wojtal, 1996; Ohmori et al., 1997) in contrast to transform faults typically ranging up to hundreds of kilometers (e.g. Wesnousky, 2005), and (3) a preferred direction of fault growth and earthquake propagation, on average, from deeper to shallower depth (e.g., McGuire et al., 2002).

On the basis of observations from modern subduction zones and ancient, exhumed accretionary complexes (e.g. Moore, 1989; Hashimoto and Kimura, 1999; Park et al., 2002a), a favored tectonic model for accretion (Fig. 1a) involves underthrusting, underplating, and translation of underplated materials along out-of-sequence-thrusts (OOSTs). In this model, trench-fill-turbiditic-sediments are partly accreted above the plate-boundary décollement, or off-scraped, at the toe of accretionary prism (e.g. Moore, 1989; Taira et al., 1991). Oceanic crust with the pelagic and clastic sediments are carried downward below the plate-boundary décollement, or underthrusted (e.g. Fisher and Byrne, 1987; Silver et al., 2001). The upper part of the underthrust section may be transferred to the overlying accretionary prism, or underplated (e.g. Platt et al., 1985; Park et al., 2002a), via duplex faulting of oceanic crust strata (Fig. 1b; Hashimoto and Kimura, 1999). Underplated materials are translated and exhumed along OOSTs that link to the master plate boundary (e.g. Morley, 1988; Kondo et al., 2005).

Kilometer-size-duplexes of oceanic crust strata in exhumed accretionary complexes, such as the Okitsu mélange in the Shimanto accretionary belt, Japan (Fig. 2b; Kanaya and Sakaguchi, 2006), are considered a product of underplating at seismogenic depth (Hashimoto and Kimura, 1999; Park et al., 2002a). Accordingly, horse-bounding thrusts of the duplex in the Okitsu mélange that juxtapose oceanic pillow basalt in the hanging walls and sedimentary rocks in the footwalls may be a segment of fossil plate-boundary décollement formed at the depth of underplating near the seismic-aseismic transition (Hyndman et al., 1997; Matsumura et al., 2003).

The purpose of this paper is to characterize the mesoscale structure (mm to tens of meters scale) of an internal horse-bounding thrust of the duplex, referred to as the Suzume fault, in the Okitsu mélange to test the tectonic model of underthrusting-

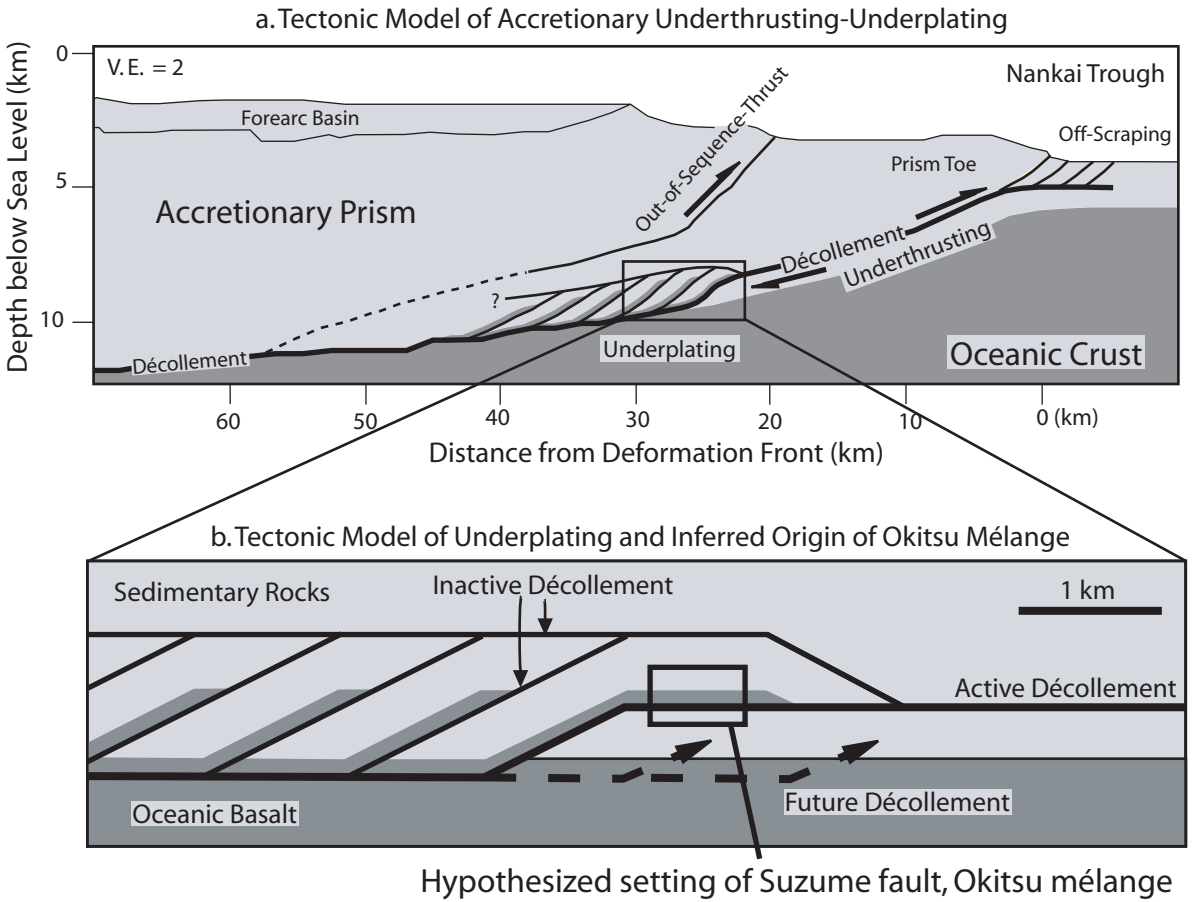

Fig. 1. Tectonic model of accretionary underthrusting-underplating and inferred origin of the Okitsu mélange, the Shimanto accretionary belt, Japan (after Park et al., 2002a, 2002b; Matsumura et al., 2003). (a) Cross-section of subduction zone and accretionary prism at Nankai Trough based on seismic imaging. Trench-fill-sediments in the subducting plate are translated, or underthrusted, beneath the plate-boundary décollement from the prism toe region to the underplating zone. Underplating occurs at depth where the décollement steps down into basalt of the oceanic crust. The sediments and the upper section of the basalt are transferred, or underplated, to the overlying accretionary prism through the formation of a duplex composed of the sediments and basalt. Underplated rocks may be uplifted along out-of-sequence-thrusts (OOSTs). (b) Schematic section of underplating regime showing duplex formation. Break-forward duplex fault development and subsequent displacement stacks horses of oceanic crust succession of oceanic basalt and sedimentary rock through updip propagation of the décollement. Horse-bounding thrusts in the duplex serve as the décollement while active, and juxtapose basalt in the hanging wall and sedimentary rock in the footwall. Hypothesized setting of the Suzume fault is shown.

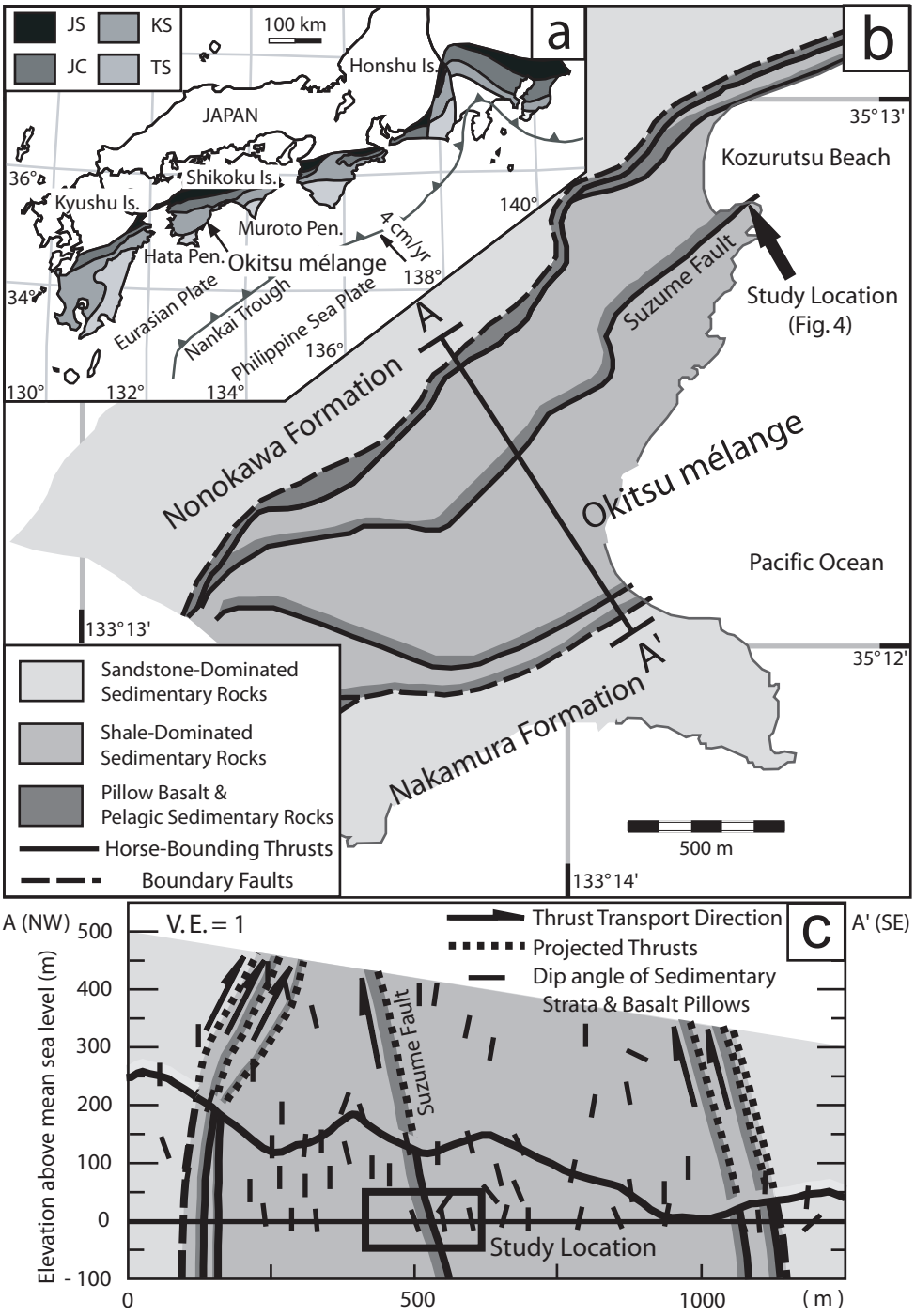

Fig. 2. (a) Map of the Shimanto accretionary complex in Japan showing the location of the Okitsu mélange. JS-Jurassic Sambagawa metamorphic belt; JC-Jurassic Chichibu accretionary complex; KS-Cretaceous Shimanto accretionary complex; TS-Tertiary Shimanto accretionary complex (Taira et al., 1988). (b) Geologic map of the Okitsu mélange, the Shimanto accretionary belt, Hata Peninsula, Shikoku, Japan (Kanaya and Sakaguchi, 2006). The Okitsu mélange is composed of km-size-duplex of oceanic crust succession of oceanic basalt and sedimentary rock. Location of the studied outcrop of the Suzume fault at Kozurutsu Beach is shown. (c) Cross section AA' of the Okitsu duplex. Location of the cross section is shown in Fig. 2b. The Okitsu duplex dips vertically, and the studied Suzume fault is locally overturned. Structural location of the study site projected in the section is shown.

underplating and to provide information on fault structure relevant to the mechanics of faulting and mechanisms of slip. According to the tectonic model, the Suzume fault is expected to be asymmetric due to dissimilar deformation paths between the hanging wall and the footwall. The hanging wall should record deformation that occurred during underplating, whereas the footwall should record deformation throughout underthrusting and underplating.

2. GEOLOGY OF THE OKITSU MELANGE AND SUZUME FAULT

A subduction complex that includes the modern Nankai subduction zone and paired metamorphic belts is present in southwest Japan (Fig. 2a; e.g. Miyashiro, 1973). The Shimanto belt, Tertiary-Cretaceous rocks metamorphosed at a low grade, is the youngest accretionary complex exposed on land, and generally considered an exhumed analogue of the modern Nankai accretionary prism (Taira et al., 1988). The Okitsu mélange is located in the east side of the Hata Peninsula of Shikoku Island, and is the most seaward and youngest mélange exposed in the Cretaceous Shimanto belt, of late Campanian to early Maastrihichian (74-70 MA) age (Taira et al., 1988; Kanaya, 2001). The Okitsu mélange is fault-bounded to the northwest and southeast by sandstone-dominated formations of the Nonokawa Formation and the Nakamura Formation, respectively (Fig. 2b; Taira et al., 1988; Kanaya and Sakaguchi, 2006.).

The Okitsu mélange constitutes a kilometer-size duplex of oceanic crust strata, in which internal thrusts stack slices (horses) of pillow basalt overlain by pelagic and shale dominated trench-fill sedimentary rocks (Fig. 2b; Kanaya and Sakaguchi, 2006). Strata and horse-bounding thrusts of the duplex in the Okitsu mélange are approximately vertical and striking NW-SE. The horse-bounding thrusts juxtapose pillow basalt in the hanging walls and sedimentary rocks in the footwalls (Kanaya and Sakaguchi, 2006). The Suzume fault, an interior horse-bounding thrust studied herein, is well exposed at Kozurutsu beach. At Kozurutsu beach, the Suzume fault displays a flat-on-flat geometry because the primary layering of the pillow basalt and of sedimentary strata are parallel to each other and to the thrust (Kanaya, 2001). The Suzume fault is locally overturned and dipping at 69° towards 182°, i.e., the basalt of the hanging wall is presently below the thrust and sedimentary rocks of the footwall (Fig. 2c).

The clastic sedimentary rocks of the Okitsu mélange display a block-in-matrix structure, which consists of sandstone boudinage in a shale matrix. The block-in-matrix structure is thought to record progressive consolidation and dewatering of partially lithified sediments during underthrusting (e.g. Fisher and Byrne, 1987; Kimura and Mukai, 1991; Ujiie, 2002). A maximum temperature and pressure of 280 ± 30 °C and

150 ± 0 MPa are estimated for the Okitsu mélange and a correlative mélange exposed in East Shikoku on the basis of vitrinite reflectance (Sakaguchi, 1996) and fluid inclusion analyses (Fig. 3; after Matsumura et al., 2003). Zircon and apatite fission track geochronology gives ages of 70 and 10 MA, respectively, for the Cretaceous Shimanto belt in Shikoku Island and records exhumation history (Hasebe et al., 1993; Tagami et al., 1995).

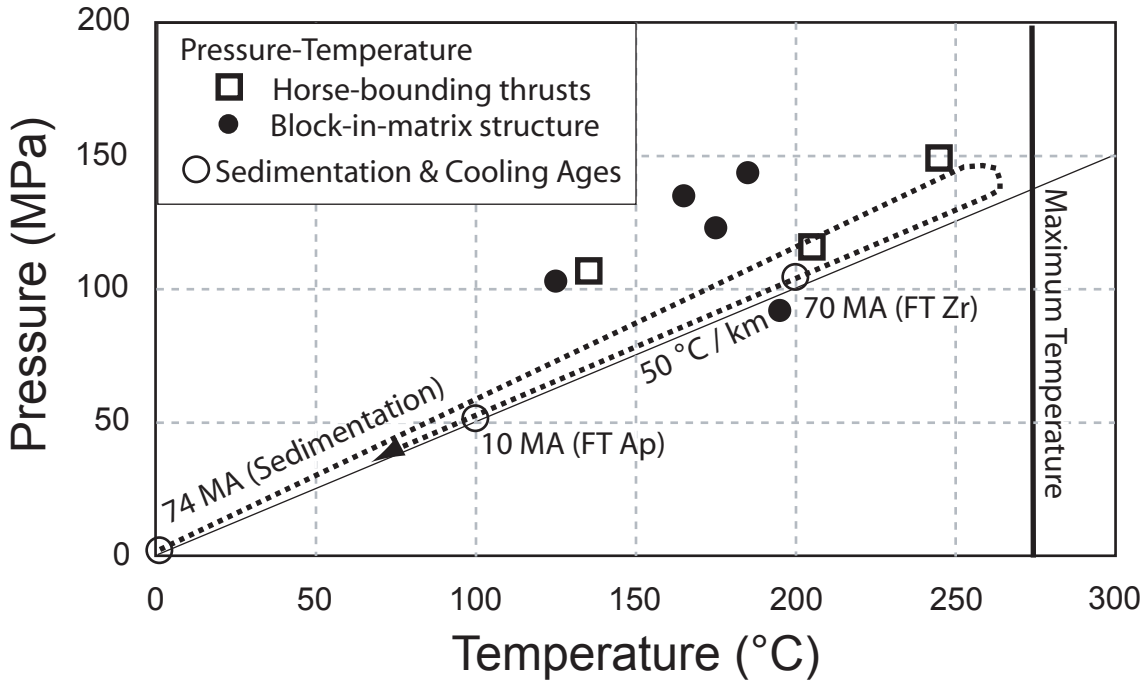

Fig. 3. Pressure-temperature-deformation-time path of the Okitsu mélange and Cretaceous Shimanto belt (after Matsumura et al., 2003; Sakaguchi, 1996; Hasebe et al., 1993; Tagami et al., 1995). Paleo pressure-temperature conditions determined based on fluid inclusion analysis from an equivalent formation of the Okitsu mélange in the Muroto Peninsula, Shikoku (Matsumura et al., 2003). Maximum paleo temperature condition determined based on vitrinite reflectance analysis from the Okitsu mélange (Sakaguchi, 1996). Times are given in million years before present. FT Zr-Zircon fission track; FT Ap- Apatite fission track.

3. METHOD

Structure and fabric of the Suzume fault was studied at a wave-cut, 80 × 100 m exposure spanning the fault at the beach. The exposure was mapped at a scale of 1:100 using surveyed reference points and locally at a scale of 1:10 using grid lines on one slip-parallel (vertical) and two slip-perpendicular (horizontal) exposures.

An industrial, hand-engine-cutter was used to cut a continuous section from the outcrop 10 meters in length, and several additional sections 20 to 60 cm in length across the fault. This was accomplished by making three 5-cm deep parallel cuts 5 cm apart in the outcrop. Twenty-cm-long sections were taken from between the cuts to recover two paired 5 × 5 × 20 cm samples. After the first sample was removed from the outcrop, a 3-mm-thick paper was glued to the side of the sample remaining in the outcrop to provide structural support to the sample during removal. Each sample was later cast in polyester resin (Reichhold, Polylite 32030-10) and then cut in two pieces: one side (1.5 cm thick) was polished for structural mapping and the other (3.5 cm thick) side was retained for future structural and chemical analyses.

Structural data, including fracture orientation and density, fracture kinematic indicators, the size and orientation of brecciated basalt pillows and sandstone boudins, and magnetic susceptibility, were collected along a 300-meter-traverse (40 meters in the hanging wall and 250 meters in the footwall) across the fault. Fracture density was determined by counting intercepts along a 25-centimeter-radius circle at each measurement location and reported as linear density (number of intercepts per meter). Fractures were classified as open or sealed (veins) and by size (mm, cm, and meter length). In addition, the density of faults greater than 1 cm in length and sub-parallel (0-30°) to the Suzume fault surface was determined. Most meter-size faults were mapped in the structural map at a scale of 1:100, and the orientation of the fault planes and slip lineation was measured. Sense of shear was determined on the basis of fracture surface morphology, using the criteria described by Hancock (1985; Goldstein and Marshak, 1988). To distinguish fault-rock units, the proportion of porphyroclast and matrix in the

outcrop was estimated using Sibson's textural classification of fault rocks (e.g. Sibson, 1977; Snoke and Tullis, 1998).

The size distribution and aspect ratio of brecciated pillow clasts were characterized on a vertical, slip-parallel exposure by measuring 10 to 20 clasts at each location. The edges of brecciated clasts were marked and photographed at the outcrop, and dimensions (long and short axes) were measured on the photographs. The long (L_1 and L_2) and short axes, and the spacing between the geometric centers of two neighboring boudins (s) in the same stratigraphic horizon were measured for 10 pairs of boudins (total 20 boudins) at each sample location. Stretch recorded by the boudinage was calculated using stretch = $2S / (L_1 + L_2)$. In addition, the volume fraction of sandstone and shale was estimated at each location.

Five measurements of magnetic susceptibility at each measurement location were taken along the 300 m traverse using a ZH instruments SM30 that uses a sensor 50 mm in diameter and oscillation frequency of 80 kHz. The instrument can record 90% of the original susceptibility in a rock as accurate as 1×10^{-7} SI Unit can be measured from inside the rock to 20 mm depth.

4. INTERNAL STRUCTURE OF THE SUZUME FAULT ZONE

The Suzume fault consists of a single, 30-m-thick zone of highly deformed rocks (Figs. 4, 5, 6). The macroscopic fault-surface, referred to as the Suzume fault surface, is defined by a distinct, centrally located, decimeter-thick ultracataclasite layer (Fig. 7) that separates deformed pillow basalts in the hanging wall and sedimentary rocks in the footwall (Figs. 8, 9). The structure of the fault zone is asymmetric in that the style of deformation in the hanging wall and the footwall is different. The fault surface is nearly parallel to the primary layering defined by sedimentary strata and elongated pillows (Fig. 10). Except for minor offsets on high-angle, secondary faults, the fault zone is continuous over the 100 m of exposure.

4.1. Hanging wall

The hanging wall consists of 30-m-thick pillow basalts overlain by 5 m of pelagic red shale with a 700-m-thick sequence of shale and sandstone (Fig. 4a). The basalt is aphanitic with 1-mm long plagioclase feldspar phenocrysts, and is dark green in the relatively undeformed portions (Fig. 9a). Red hydrothermal chert occasionally is present as quartz veins within or between the pillows. In undeformed regions, the basalt pillows range from 4 to 50 cm in diameter, and are somewhat elongate parallel to stratigraphic layering (Fig. 8a).

Fault-related damage is defined by an increase in fracture density and decrease in the size of fractured pillow clasts towards the ultracataclasite (Fig. 11). For all mesoscale fractures, linear density increases progressively from 200 to 300 towards the ultracataclasite layer (Fig. 11a), but fracture density varies with apparent fracture length along the traverse. Faults with length greater than centimeters and subparallel to the Suzume fault surface display a more distinct increase in linear density from 10 to 50 over a 10-m-thick zone adjacent to the ultracataclasite (Fig. 11b). Millimeter-thick veins, mostly with calcite fill, occur throughout the hanging wall and do not appear to vary in density as a function of distance from the ultracataclasite (Fig. 11f). Over the zone of fault-related features, there is a decrease in the size of fractured pillow clasts towards the

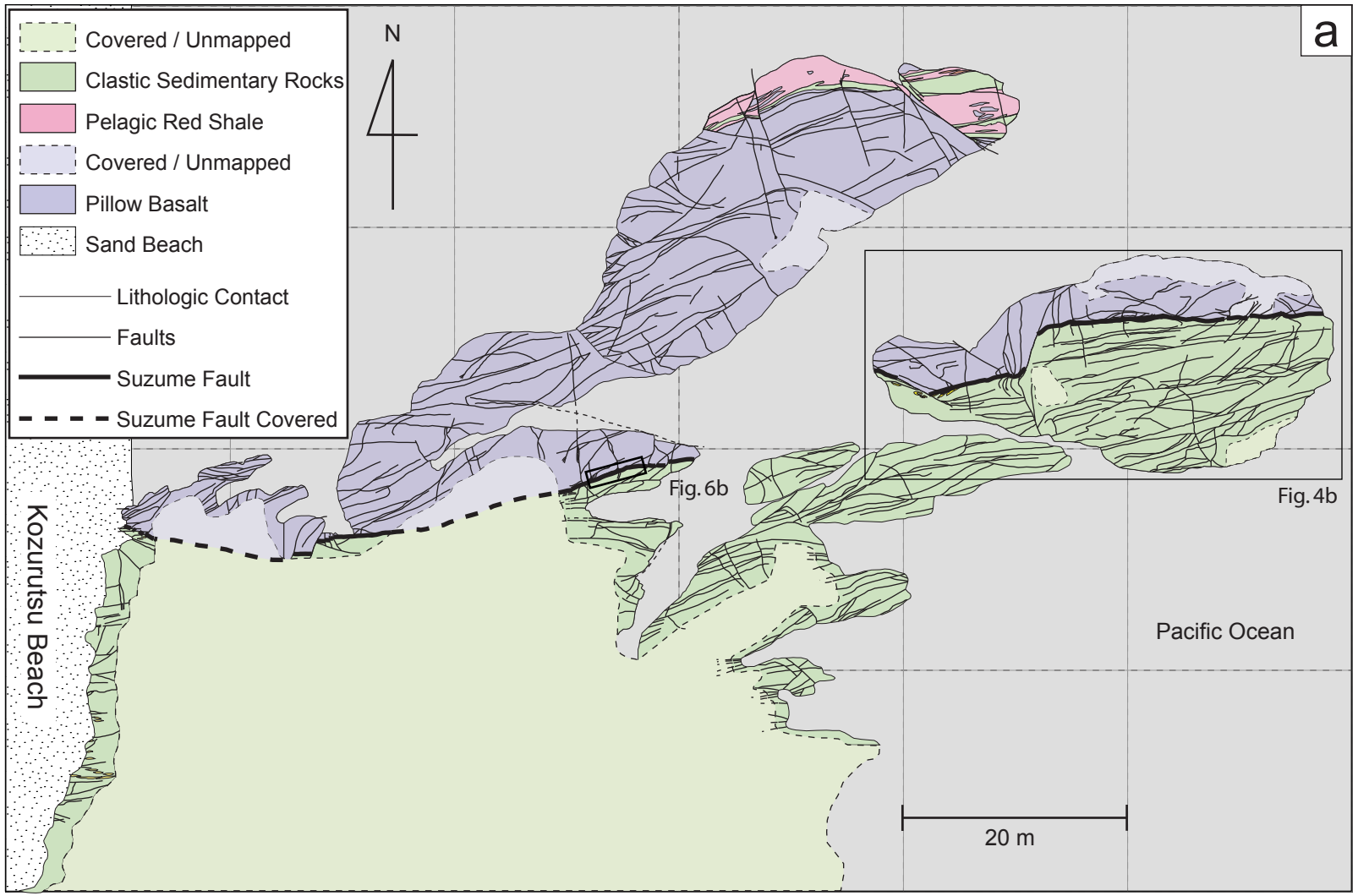

Fig. 4. (a) Outcrop map of the Suzume fault exposure at the Kozurutsu Beach study location showing lithology and faults mapped at a scale of 1:100. Location of enlarged map (Fig. 4b) and a detailed map (Fig. 6a) is shown. (b) Enlarged map showing distribution of fault rocks. Location of the fault detailed maps (Fig. 5 and Fig 6b) are shown. Both (a) and (b) are oriented approximately perpendicular to the Suzume fault surface and thrust direction.

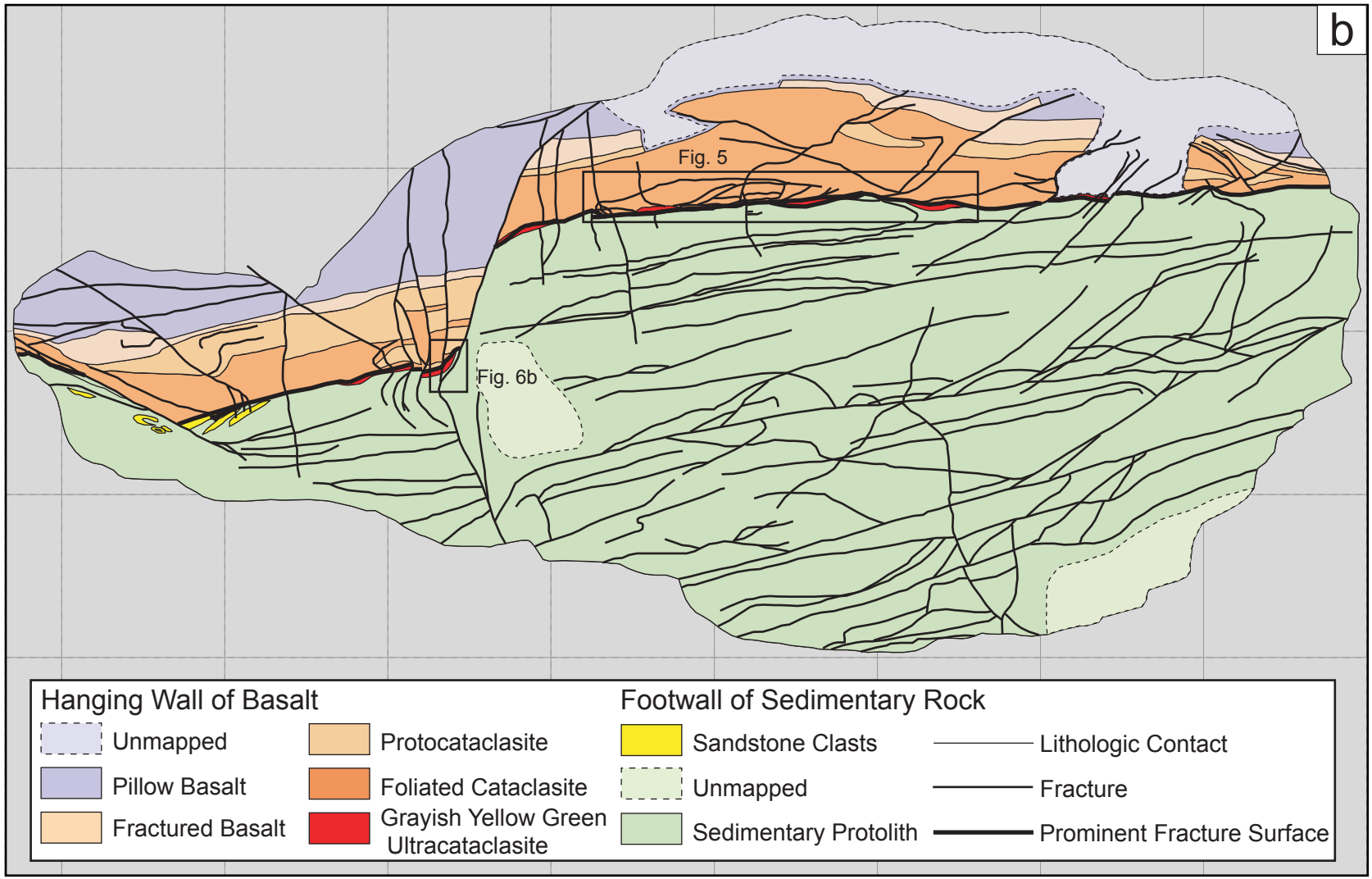

Fig. 4 (continued).

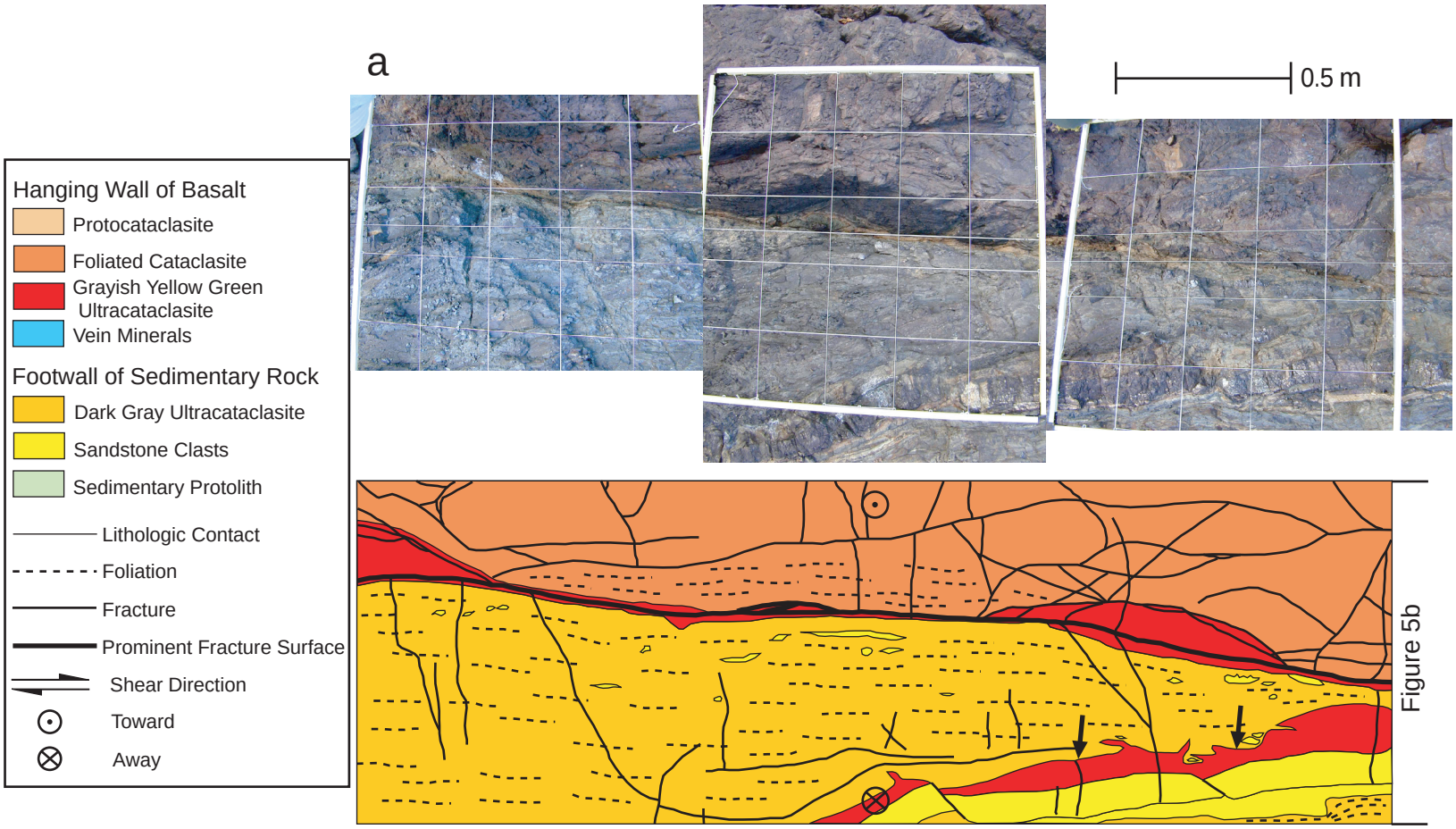

Fig. 5. Detailed structure of the central ultracataclasite layer in the Suzume fault on a slip-perpendicular exposure mapped at a scale of 1:10. Basalt of the hanging wall at the top and sedimentary rock of the footwall at the bottom. Grid in the photos is 20 cm. Locations of the map is shown in Fig. 4b. (a) Eastern and (b) Western half of the map. Arrows indicate slivers, patches, and porphyroclasts of ultracataclasite and the ultracataclasite contact displaying interfingering geometry. Mesoscale fault curves towards the Suzume fault surface, branches out, and dissipates (circle).

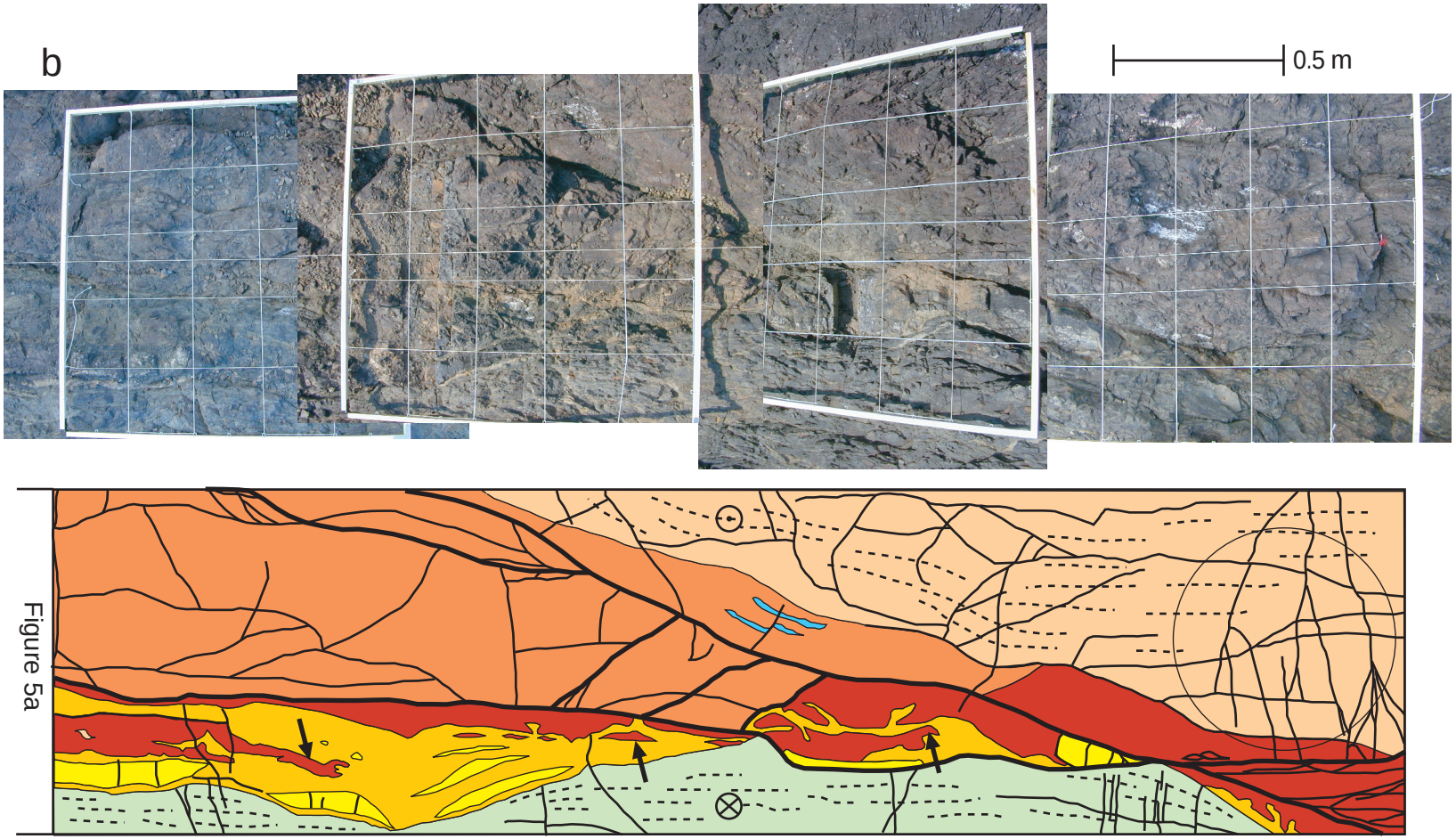

Fig. 5 (continued).

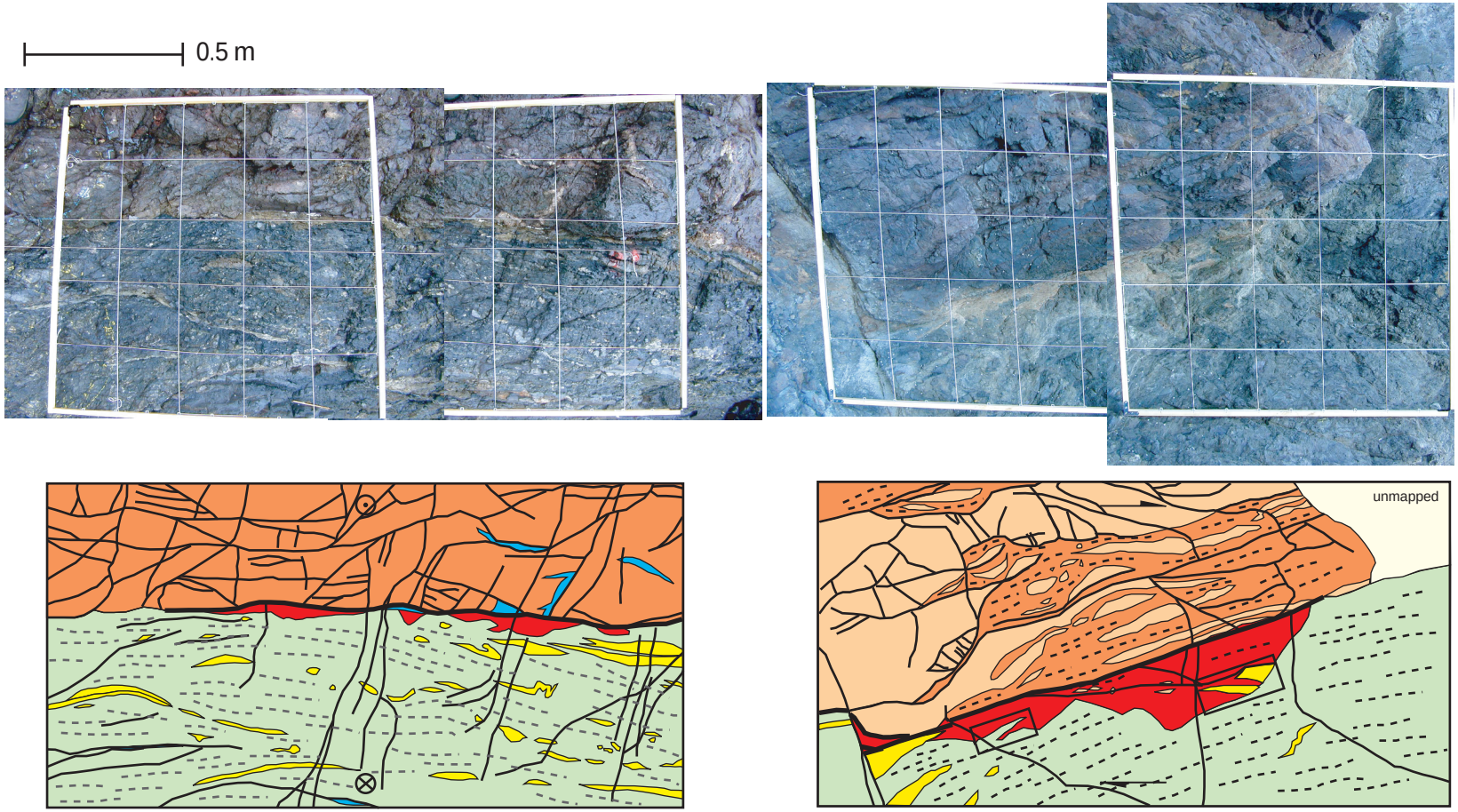

Fig. 6. Detailed structure of the central ultracataclasite layer in the Suzume fault on (a) slip-parallel and (b) slip-perpendicular exposures mapped at a scale of 1:10. Basalt of the hanging wall at the top and sedimentary rock of the footwall at the bottom. Grid in the photos is 20 cm. Locations of the maps are shown in Fig. 4. Wedge-like protrusion of ultracataclasite into the sedimentary rock is noted (boxes). Keys and symbols are the same as Fig. 5.

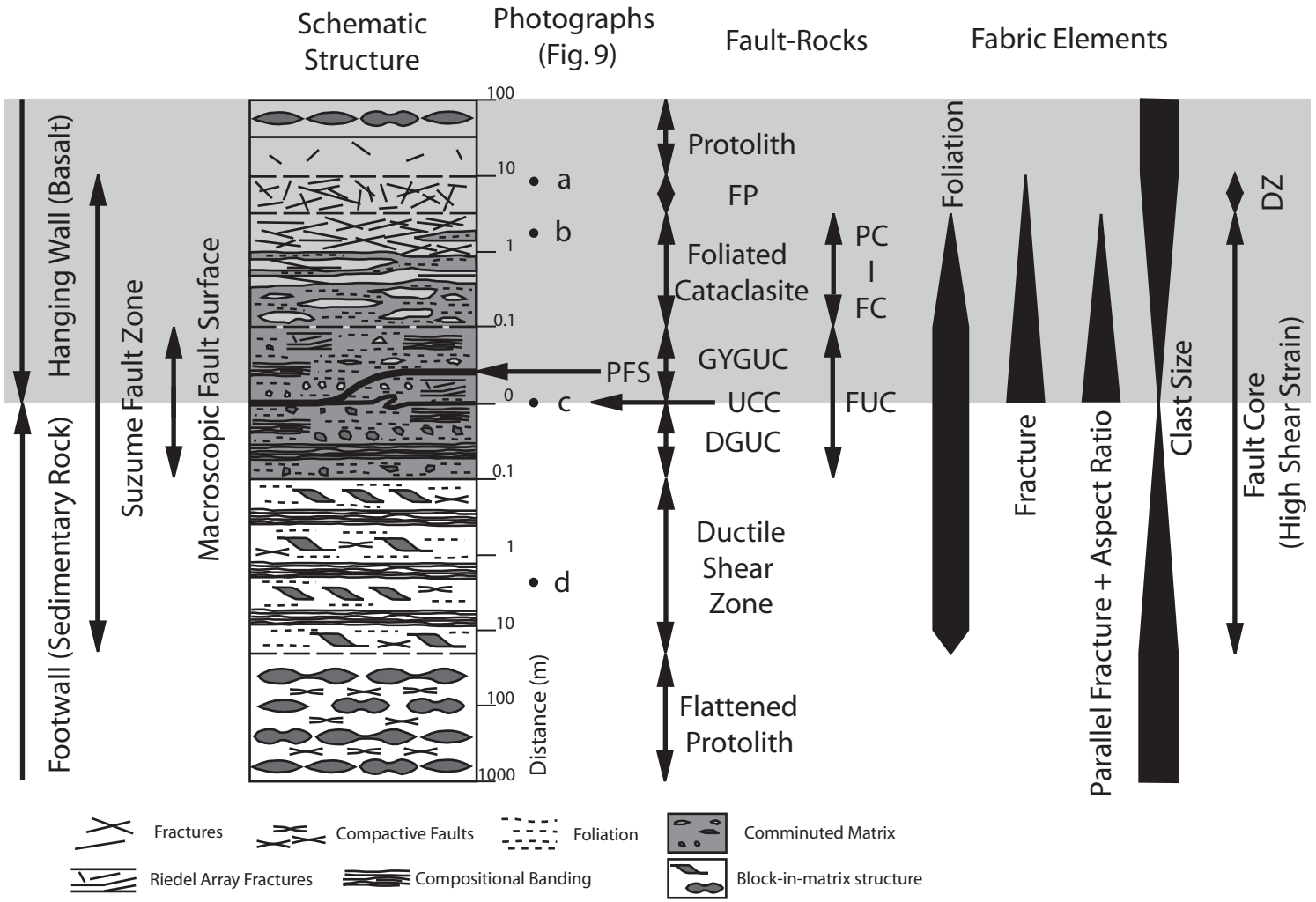

Fig. 7. Synopsis of structural elements of the Suzume fault, Okitsu mélange. Distance is measured from the contact between the grayish yellow green ultracataclasite and dark gray ultracataclasite. Location of samples in photographs in Fig.9 is indicated by letter a-d. The extent of each structural element is defined on the basis of fault rock textures (Fig. 8 and 9) and fabric element measurements (Fig. 11 and 13). The damage zone and core of the fault zone are determined based on fault-related deformation and shear accommodation, respectively. UCC-Ultracataclasite contact; PFS-Prominent shear fracture surface; FP-Fractured protolith; GYGUC-Grayish yellow green ultracataclasite; DGUC-Dark gray ultracataclasite; PC-Protocataclasite; FC-Foliated cataclasite; FUC-Foliated ultracataclasite; DZ-Damage zone.

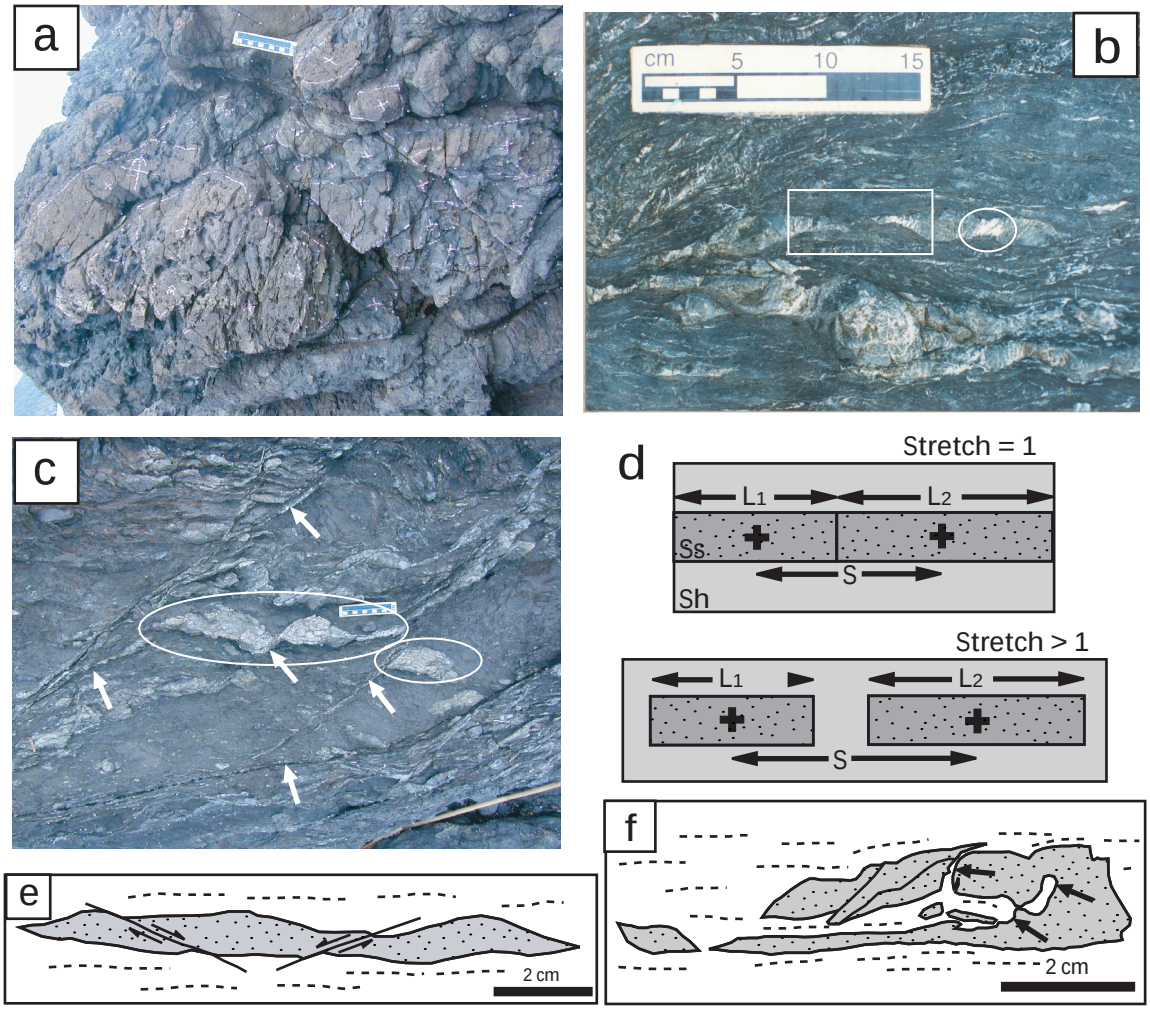

Fig. 8. Structure of protoliths illustrated in photographs and diagrams. Photos and diagrams are oriented perpendicular to the primary layering of pillow basalt and sedimentary rocks and parallel to the direction of elongation. (a) Relatively undeformed pillow basalt representation of the protolith. The bar scale is 10 cm. (b) Photograph of the fault-flow type (box) and joint-flow type (ellipse) boudinage. In the fault-flow type, shale matrix and sand boudins are disrupted by flow and fault planes at low angles to the sedimentary layering, respectively. In the joint-flow type, high-angle fractures and normal faults filled with minerals are developed in the pinch and edge portions of sand boudins, whereas the shale matrix is deformed by flow. (c) Fault-fault type. The bar scale is 10 cm. Sand boudins and shale matrix (ellipses) are disrupted by faults (arrows) at low angles (0-45°) to the sedimentary layering. The bedding of sand and shale is dragged into fault plances. (d) Schematic diagram showing quantification of stretch from boudinage geometry where stretch = $2S / (L_1 + L_2)$. Stretch is determined by the spacing of two neighboring boudins, S, over the average lengths of the two boudins, L_1 and L_2. Sh: Shale, Ss: Sandstone. Failure of sand layers is assumed to be by high-angle fractures, and internal flow of the sand is neglected. (e) Sandstone layer extended by a conjugate pair of faults at low angles to the layering in the fault-flow type of boudinage. (f) Flow-flow type. Shale matrix is intruded into sand boudins (arrows).

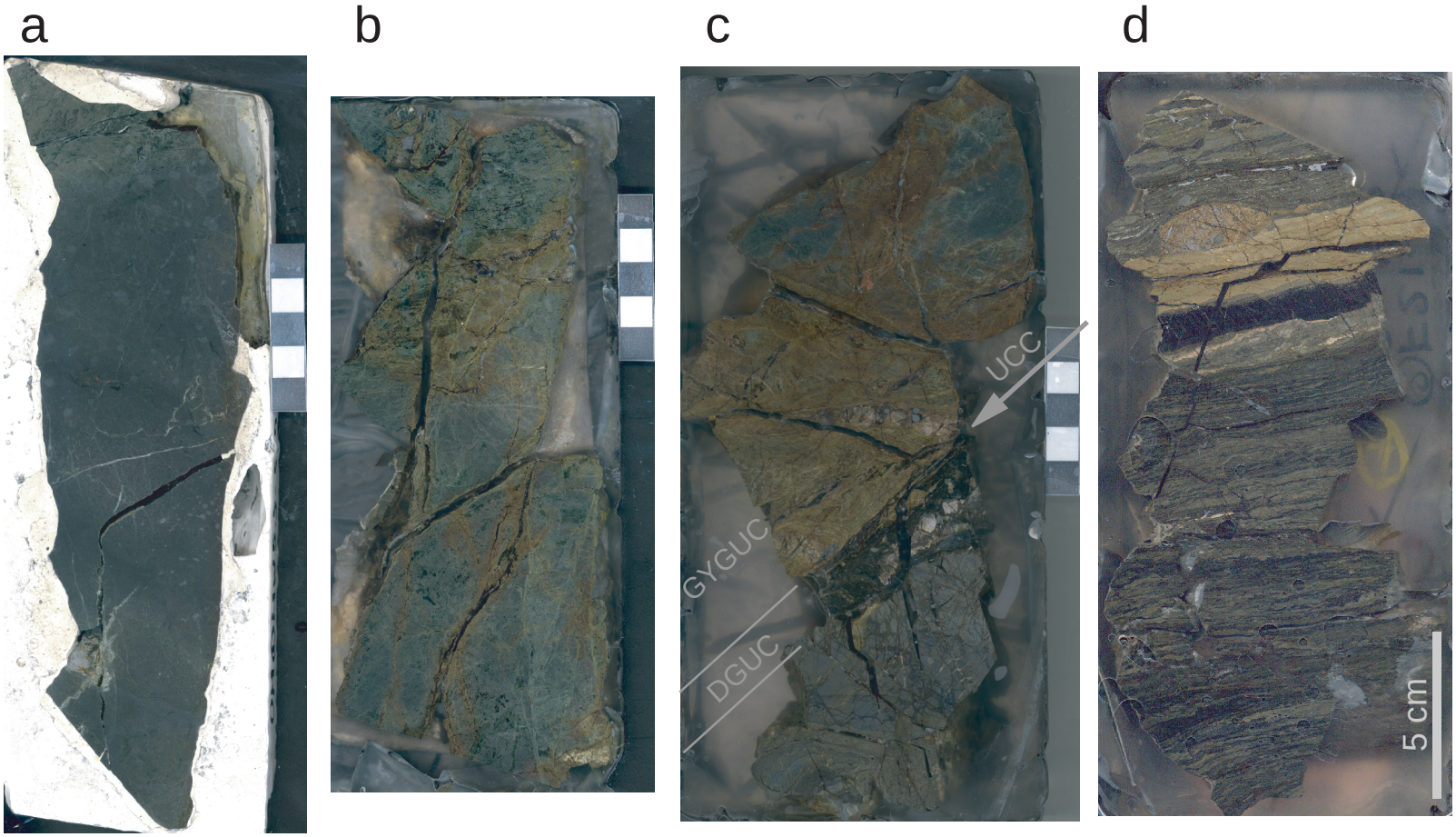

Fig. 9. Photographs of polished samples of rock from the Suzume fault zone. Polished surfaces are oriented perpendicular to the macroscopic fault-surface and parallel to the thrust direction; cm bar scale shown. Location of samples is shown in Fig. 7. (a) Relatively undeformed pillow basalt 5.5 m from the ultracataclasite contact in the hanging wall. (b) Protocataclasite derived from basalt 2.1 m from the ultracataclasite contact in the hanging wall. (c) The ultracataclasite contact (UCC) separating the gray yellowish green ultracataclasite (GYGUC) from basalt (above) and the dark gray ultracataclasite (DGUC) from sedimentary rock (bottom). (d) Foliated fault rock from the ductile shear zone 2.0 m from the ultracataclasite contact in the footwall.

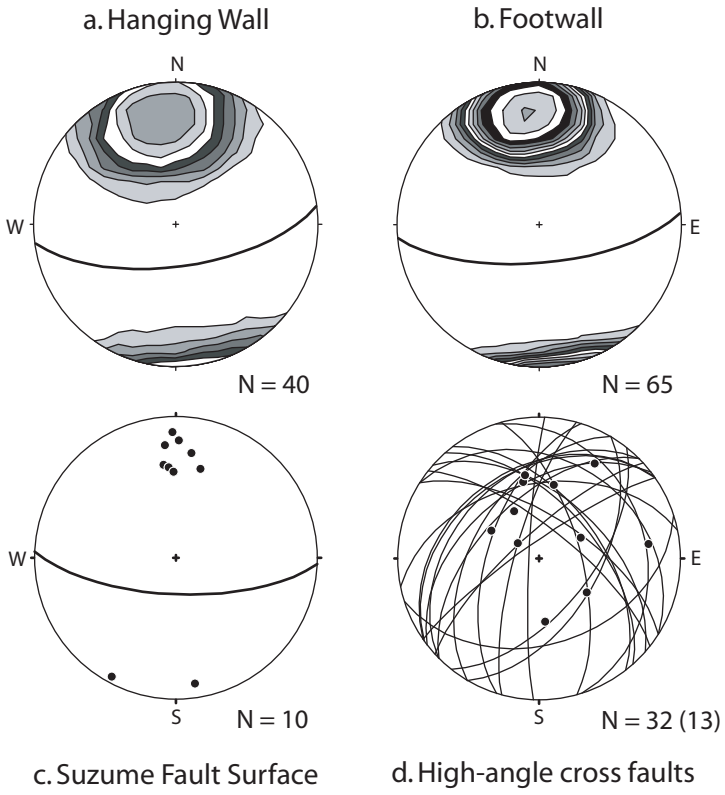

Fig. 10. Orientation of primary layering in the host rocks, the Suzume fault surface, and of late-stage mesoscale cross faults. Lower-hemisphere, equal-area projections with N at top. Contoured using the Kamb method with two sigma contour interval. Number of data is indicated. Normals to planar features are shown by contours or dots, and the mean orientation of the plane structure is shown by great circles. Layering in (a) hanging wall defined by basalt pillows and (b) footwall defined by sedimentary bedding. (c) The contact surface of the grayish yellow green ultracataclasite and dark gray ultracataclasite. The orientation of the ultracataclasite contact is assumed to represent that of the macroscopic, Suzume fault surface. (d) Mesoscale faults that offset the ultracataclasite layer shown by great circles and slip lineation shown by dots.

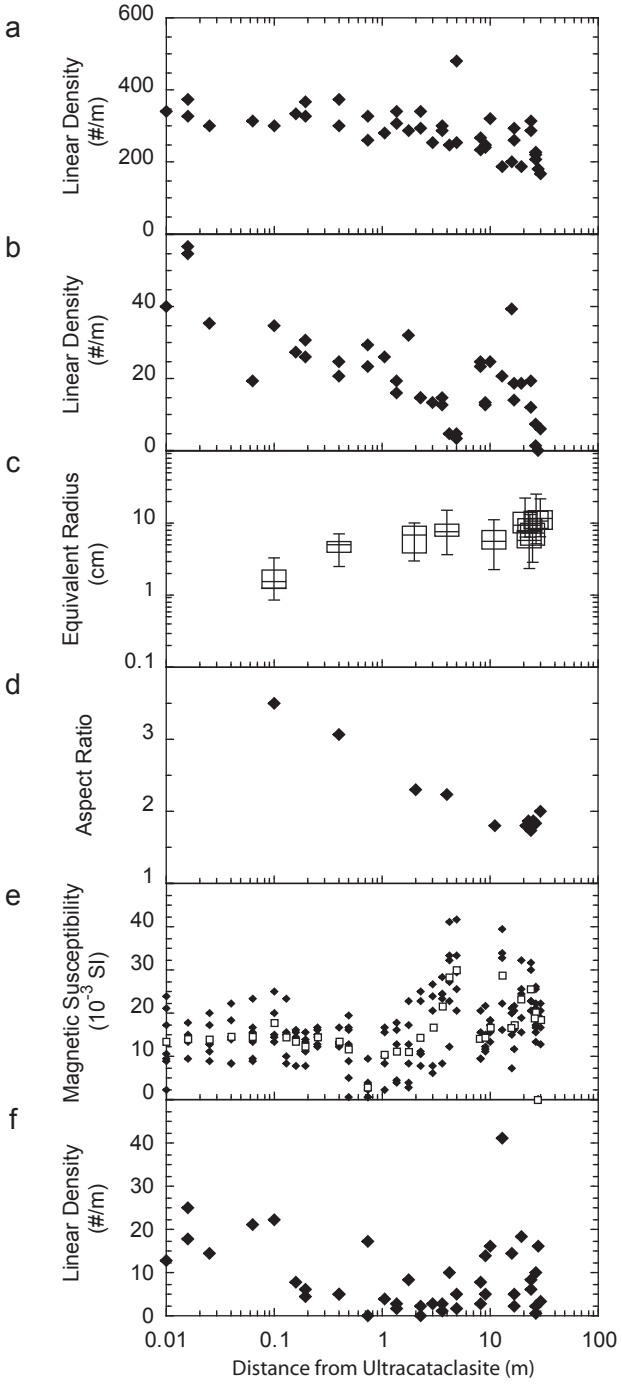

Fig. 11. Structural elements in the hanging wall as a function of distance from the ultracataclasite contact. Distance is measured perpendicular to the Suzume fault surface. (a) Linear density of all mesoscale fractures. (b) Linear density of faults that are greater than centimeters in length and sub-parallel (up to 30°) to the Suzume fault surface. (c) The size distribution of fractured basalt pillows based on 10 to 20 measurements at each measurement station. Boxes encompass the middle 50% of data; intermediate line in the box is the median; whiskers show the range 1.5 times of the length of the box from the box end, or the maximum data within the range if any. (d) The mean aspect ratio of fractured basalt pillows. The aspect ratio is determined by the ratio of long to short axes of the clasts at each measurement station. (e) Magnetic susceptibility. At least 5 measurements were done at each measurement station by repeating the sampling traverse. The open squares are the mean value at each location. (f) Linear density of veins.

ultracataclasite, and an increase in aspect ratio corresponding to the change in the shape of clasts by fracture from nearly equi-dimensional undeformed pillows, to lenticular and tabular clasts near the ultracataclasite (Fig. 11c, d).

Within an innermost zone of intense fracture, the development of cataclastic rocks, foliations, and color change are profound (Fig. 4b). The inner zone of cataclastic rocks is continuous along the Suzume fault surface and 5 m thick on average, but displays significant variation in thickness. The cataclasite layer forms a gradational boundary with the fractured basalt, and the intensity of cataclasis increases towards the ultracataclasite. The progressive deformation is characterized by an outermost 3-m-thick layer of dark maroon protocataclasite, an intermediate 2 to 3-m-thick layer of light green cataclasite, and finally a 10 to 30-cm-thick layer of gray yellowish green ultracataclasite (Fig. 9). Foliation defined by the alignment of the lenticular porphyroclasts and mm-scale compositional banding is pronounced in the cataclasite and ultracataclasite, and is always parallel to the Suzume fault surface in both vertical and horizontal exposures. Cataclasite may be locally present within the protocataclasite, but the grayish yellow green ultracataclasite is always adjacent to the contact with the footwall (Figs. 5, 6).

Magnetic susceptibility is variable in the hanging wall, but shows a gradual decrease from 40×10^{-3} SI at 5 m, to 0.1×10^{-3} SI at 0.5 m, and then remains at 8 to 20×10^{-3} SI within 0.5 m of the ultracataclasite (Fig. 11e).

The mesoscale faults are predominantly oriented subparallel to the Suzume fault surface, but are comprised of two distinct subsets. Both subsets strike parallel to the fault surface. One subset dips to the south, very nearly parallel to the fault surface, whereas the other dips to the north (Fig. 12a, c). Faults of these two subsets are mutually crosscutting and show a preferred orientation of steeply plunging slickenlines. The B-axes, imaginary lines mutually perpendicular to both slickenlines and poles to fault planes, form a point maximum that slightly plunges to the west (Fig. 12b). Because the majority and mean orientation of faults with known sense-of-shear synthetic and antithetic to the thrusting direction of the Suzume fault primarily occur in the parallel and subparallel subsets, respectively, all faults in the two subsets are assumed to be

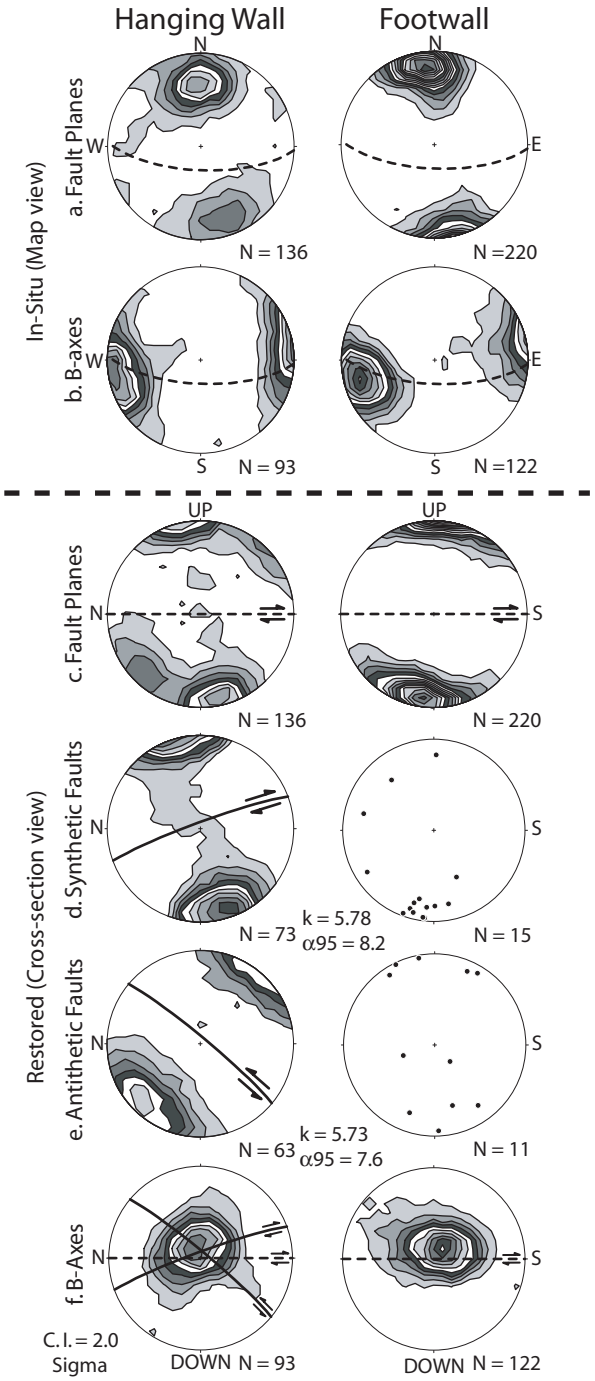

Fig. 12. Fabric of mesoscale faults in the hanging wall (left column) and footwall (right column). Lower-hemisphere, equal-area projections. (a–b) fabric in-situ data and projections onto horizontal plane with N at top. (c–f) fabric data rotated to restore that to hypothesized original horizontal order and projections onto plane perpendicular to the Suzume fault surface and parallel to the thrust direction (cross section view). Number of data is indicated. Contoured using the Kamb method with two sigma contour interval. Great circles show the mean orientation of the Suzume fault surface (dashed), synthetic faults, and antithetic faults with arrows indicating the sense-of-shear (solid). (a, c) Normals to fault planes for all mesoscale faults, (b, f) B-axes of faults, (d) synthetic faults (right-lateral sense-of-shear) and (e) antithetic faults (left-lateral sense-of-shear). k and $\alpha 95$ are concentration factor and confidence cone for the mean orientation, respectively.

synthetic and antithetic to the thrusting (Fig. 12d, e). If true, the faults in the two subsets constitute a quasi-conjugate fault set, consistent with contraction at low angles to the Suzume fault surface (Fig. 12f). An additional, minor set of faults displays a preferred orientation at large angles to the fault surface (Fig. 12a). Some of these faults offset the ultracataclasite and other fault-rock units as well as the quasi-conjugate faults (Fig. 10d).

4.2. Footwall

The footwall protolith consists of interbedded shale and sandstone that has undergone distributed deformation throughout the entire sedimentary section of the Okitsu mélange. The interbedded sandstone and shale displays a block-in-matrix structure, consisting of sandstone boudins in a shale matrix, described as boudinage in general (e.g. Ramberg, 1955; Ramsay, 1967; Goscombe et al., 2004). The stratigraphic section displays variation in proportion of sandstone to shale (Fig. 13a). Assuming that sand layers and boudins did not undergo change in thickness by flow, and that the short axis of sandstone boudins represents the original thickness of sand layers, sandstones are thicker bedded and more dominant 120 to 20 m from the ultracataclasite, whereas shale with thinner sandstone layers is more dominant within 20 m of the ultracataclasite (Fig. 13b, c).

The block-in-matrix structures are variable in style (e.g. Needham, 1995), but can be grouped into four styles based on the failure mode of the sandstone boudins and of the shale matrix: flow-flow, fault-flow, fault-fault, and joint-flow (Fig. 8). In the flow-flow type, the boundaries between boudins and matrix are undulatory, and mm-size clasts of sandstone are distributed throughout the shale between boudins, and shale intrudes into the boudins. The failure surfaces of sand layers are variable in orientation and range from 0° to 90° to the sand layering. The separation of the boudins ranges up to a decimeter. The failure mode of this type is similar to that of the drawn boudinage (Goscombe et al., 2004). In the fault-flow type, the edges of boudins are defined by shear surfaces at low angles (< 30°) to the sandstone layering, which display sense-of-shear consistent with layer-normal flattening. The shale between neighboring boudins

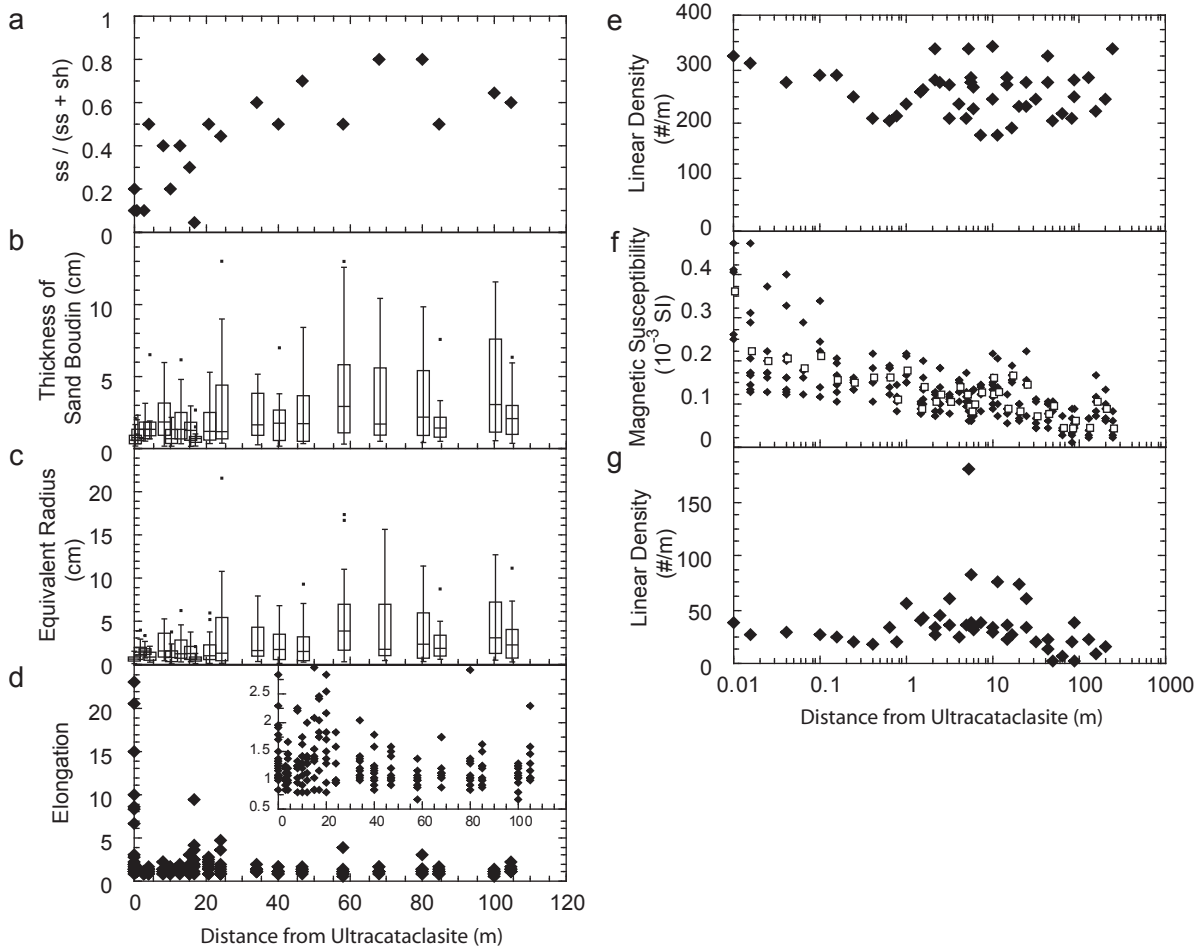

Fig. 13. Lithology and structural elements in the footwall as a function of distance from the ultracataclasite contact. Distance is measured perpendicular to the Suzume fault surface. (a) The volume fraction of sandstone (ss) in interbedded shale (sh) and sandstone. (b) The thickness of sand boudins. Thickness is assumed to represent original sandstone layer thickness (see text). (c) The size distribution of sandstone boudins represented by equivalent radius. Keys for the box plots are the same as Fig. 11, except dots show extrema (data beyond 3 times of the length of the box from the box end). (d) Stretch of the sedimentary layers. Inset shows distribution of boudins with small stretch. 10 pairs of boudins (total 20) are measured at each sample location. Stretch quantified as described in text and in Fig 8d. Although indeed elongated at the outcrop, less than 1 of stretch is due to overlap of boudins across failure surfaces and lengthened boudin long axes, resulted from failure of sand layers by low angle normal faulting and by internal flow. (e) Linear density of all mesoscale fractures. (f) Magnetic susceptibility. At least 5 measurements were done at each measurement station by repeating the sampling traverse. The open squares are the mean value at each location. (g) Linear density of veins.

shows distributed flow without macroscopic fracture. The separation of boudin ranges up to a cm. This type is similar to the extensional shear fracture (Mandal et al., 2000) or shear band (Goscombe et al., 2004) boudinage. In the fault-fault type, both boudins and matrix are offset along discrete shear surfaces oriented at an angle of 45° to the layering, and the sense-of-shear is again consistent with layer-normal flattening. Sedimentary layering shows drag-folding near slip surfaces, and the slip surfaces terminate within the matrix. Secondary minerals may be precipitated along slip surfaces. The separation of boudins ranges up to a cm. In the joint-flow type, mineralized joints and faults approximately perpendicular (70-90°) to the sand layers increase in density towards the center of the pinch. The shale surrounding the boudins show distributed flow without macroscopic fractures. The separation of boudins ranges up to a few mm. This type is similar to the tensile fracture (Mandal et al., 2000) or torn (Goscombe et al., 2004) boudinage.

The relationship between the boudinage style and lithology or structural position relative to the Suzume fault is not clear; however, stretch recorded by the boudinage does vary with distance from the ultracataclasite (Fig. 13d). The alignment of boudins is chiefly parallel to the sedimentary layering, and some are asymmetric, displaying an S-C type composite planar fabric. More than 20 m from the fault, the sedimentary rocks are characterized by fairly uniform stretch at 0.7 to 2.0 with large boudin size and aspect ratio (Fig. 13b-d). Larger stretch of 0.8 to 5.0 with non-uniform distribution and small boudin size and aspect ratio occurs within 20 m of the ultracataclasite. Extreme stretch of 1 to 25 with very small clast size and nearly equi-dimensional shape is observed within 0.2 m from the ultracataclasite. The boudinage appears to display no significant difference in stretch between vertical and horizontal exposures.

Neither mesoscale fractures nor vein minerals significantly increase in density towards the ultracataclasite (Fig. 13e, g). In addition to vein minerals precipitated along the longer fractures that penetrate sedimentary layers, vein minerals along numerous, distributed fractures less than centimeter in length that are contained within sandstone layers are characteristic throughout the sedimentary section. Wavy, scaly cleavages,

aligned parallel to the sedimentary layering, are present in shale throughout the sedimentary section, and the cleavage surfaces are coated by clay minerals. Foliation defined by mm thick compositional banding is characteristic within 20 m from the ultracataclasite (Fig 9d). Folds, a few dm in wavelength and amplitude, occasionally occur elsewhere in the footwall. Sheath folds, a few m in size, and isoclinally folded boudins are developed at locations within 2 to 3 m from the ultracataclasite. Pronounced drag-folding of sedimentary beddings without mesoscale fractures often occurs along mesoscale fault planes throughout the sedimentary section (Fig. 8c).

A 2 to 30-cm-thick layer of dark gray ultracataclasite with angular to well-rounded clasts composed of sandstone, siliceous shale, and fragmented veins generally is present along the contact with the gray yellowish green ultracataclasite of the hanging wall (Fig. 9c). The dark gray ultracataclasite is also distinguished by the abrupt and extreme change in stretch relative to the sedimentary rocks more distant from the ultracataclasite. Except for variation in protolith lithology, no significant change in color is observed with distance from the ultracataclasite into the footwall. Magnetic susceptibility progressively increases from 0.06–0.18 $\times$ 10^{-3} SI at distance to 0.1–0.48 $\times$ 10^{-3} SI towards the ultracataclasite (Fig. 13f).

Mesoscale faults have preferred orientations with a dominant set parallel to the Suzume fault surface (Fig. 12a, c). Based on the presence of faults with opposite sense of shear in this set, the faults can be groped into subsets that are synthetic and antithetic to the thrusting direction of the Suzume fault (Fig. 12d, e). Faults of the two subsets are mutually crosscutting, and the B-axes show a point maximum concentration and plunge 15° to the West (Fig. 12b). Assuming that the faults in the dominant set constitute a quasi-conjugate geometry similar to the outcrop scale conjugate faults (Fig. 8e), contraction normal to the sedimentary layering is indicated. The distributed faults contained within sand layers verge oppositely, displaying conjugate pairs, at angles of 30-45° to the sedimentary layering. Similar to the high-angle faults in the hanging wall, a few high-angle faults are present in the footwall and cut all other structure.

4.3. Central ultracataclasite layer

The ultracataclasite layer generally consists of two types of ultracataclasite, a grayish yellow green (5GY 7/2) ultracataclasite associated with the pillow basalt and a dark gray (N3) ultracataclasite associated with the sedimentary rocks (Figs. 5, 6). A through-going, prominent shear fracture surface (PFS), smoother than other mesoscale faults in the fault zone, is locally present within the ultracataclasite layer. The structure of the ultracataclasites, the PFS, and the contact between the two ultracataclasites (the ultracataclasite contact), vary considerably along the strike (Table 1). For many locations, the ultracataclasite contact is undulatory and interfingering, in which slivers of both types of ultracataclasites up to a few meters in length and 10 cm in width are interlayered. In a few locations, the ultracataclasite contact occurs at the PFS. Nonetheless, a narrow layer of ultracataclasites is present along the contact between basalt and sedimentary rocks, over at least 100 m, in the studied outcrop.

The contact of the grayish yellow green ultracataclasite with the surrounding cataclasite (e.g. pale brown 5YR 5/2, red purple 5RD 6/2) is transitional, and characterized by a gradual change in the size of fractured pillow clasts (Fig. 11c). The dominant porphyroclasts within the grayish yellow green ultracataclasite are of basalt, but a few slivers and clasts of the grayish yellow green ultracataclasite, up to a decimeter in length, are found in the dark gray ultracataclasite. Some shear surfaces in the orientation of P and R1 shears of the Riedel array are evident in the polished samples of the grayish yellow green ultracataclasite, and are distinguished by presence of layers of black ultracataclasite (Fig. 9c).

The dark gray ultracataclasite layer is always in contact with surrounding sedimentary rocks, but a distinct contact is difficult to identify if the bounding sedimentary rock is shale because of the similar color and particle size. Angular porphyroclasts of sedimentary rocks are always confined into the dark gray ultracataclasite layer. Within lenticular porphyroclasts in the layer, small shear occurs as conjugate pairs with a dihedral angle of 40° and implies contraction direction normal to the Suzume fault surface.

Table 1

Location of prominent shear fracture surface (PFS) in the ultracataclasite layer of the Suzume fault, Okitsu mélange.

Map	Length (m)	Fraction of PFS in different locations (%)				
		GUC/Basalt	within GUC	GUC/DGUC	within DGUC	Not Present
Fig. 5	7	42	43	15		
Fig. 6a	2	90			10	
Fig. 6b	2	60		20		20
Total	11	54	27	13	2	4

GUC = Grayish yellow green ultracataclasite; DGUC = Dark gray ultracataclasite.

GUC/Basalt indicates PFS is located between GYGUC and basalt.

GUC/DGUC includes the boudanry between basalt and sedimentary rock.

All structures in the ultracataclasite layer are truncated by the PFS, except for the high-angle mesoscale faults that offset the ultracataclasite layers and bounding damaged rock. The PFS is well developed in the east side of the study area (Figs. 5, 6a), extends for at least 40 meters before it becomes difficult to distinguish to the west (Fig. 6b). If present, the PFS is located primarily within the grayish yellow green ultracataclasite or between the grayish yellow green ultracataclasite and the surrounding cataclastic basalt (Table 1). In a couple locations, a short section of the PFS forms at the ultracataclasite contact or is located between the dark gray ultracataclasite and surrounding sedimentary rock. Although the grayish yellow green ultracataclasite is fairly cohesive, the ultracataclasite directly adjacent to and within a few cm from the PFS is less cohesive and has a light yellowish green to brownish green color. The PFS is mostly a single surface, but locally branches into a few surfaces (Fig. 5b).

The proportion of porphyroclasts to matrix is variable for both types of ultracataclasites, but on average 10-20% by volume of the ultracataclasite is porphyroclasts. Porphyroclasts range up to several mm in size in the grayish yellow green ultracataclasite and up to dm in size in the dark gray ultracataclasite. Smaller porphyroclasts are equi-dimensional, whereas larger porphyroclasts tend to be lenticular. Some porphyroclasts are composed of older ultracataclasite. Although mesoscale veins are not numerous, vein fragments mm in diameter occur within the layers. Foliation defined by the alignment of multiple porphyroclasts and porphyroclast shape preferred orientation is well developed throughout the ultracataclasite layers and is oriented parallel to the Suzume fault surface (Fig. 9c). Some porphyroclasts in the layers display δ and σ types of asymmetric tails (Passchier and Simpson, 1986) consistent with thrusting, i.e., a shear of the basalts upward relative to the sedimentary rocks.

A wedge of sedimentary rock, 0.2 m in length and 0.1 m in thickness, protrudes into the grayish yellow green ultracataclasite and is oriented parallel to the Suzume fault surface (Fig. 6a). In addition, dark gray ultracataclasite is observed to form a 2-cm-thick intrusion into the sedimentary rock along a mesoscale fault that cuts the ultracataclasite but is offset by the PFS. A few mesoscale faults in the hanging wall that cross the

ultracataclasite layer curve into an orientation perpendicular to the layer, and branch into several surfaces as the ultracataclasite layer is crossed, and ultimately dissipate in the sedimentary host rock (Fig. 5b).

5. STRUCTURAL EVOLUTION OF THE SUZUME FAULT ZONE

5.1. Environment of thrusting

Underplating through the formation of a duplex is indicated by a downward step of the décollement towards the hinterland as seen in the seismic profiles from the modern Barbados (Westbrook et al., 1982) and Nankai subduction zones (Park et al., 2002a). In Nankai, underplating appears to occur at depth of 5 km below the sea floor and 30 km from the toe (Park et al., 2002a), and on the basis of thermal modeling at a P-T condition of 150 MPa and 300 °C (Hyndman et al., 1997). The maximum paleo-pressure-temperature condition determined for the Okitsu mélange (Fig. 3; Sakaguchi, 1996; Matsumura et al., 2003) is compatible with the expected conditions of modern duplex underplating. Additionally, the timing of underthrusting, underplating, and the initiation of uplifting in the Okitsu mélange, as indicated by the extreme short period between the sedimentation (Taira et al., 1988) and exhumation ages (Hasebe et al., 1993; Tagami et al., 1995), suggests that underplating and duplexing occurred at about the maximum burial depth and temperature (4-6 km, 149 ± 0 MPa; Matsumura et al., 2003, 280 ± 30 °C; Sakaguchi, 1996) over a time span of a few million years. The km size duplex-structure of the Okitsu mélange, as well as the structural setting and the burial-exhumation history, suggests that the horse-bounding thrusts of the duplex in the Okitsu mélange are the product of underplating, and that the Suzume fault was a segment of a plate-boundary décollement of a subduction zone.

Assuming a typical break-forward model for duplex development, and that the cutoff angle of thrusts relative to the roof and floor thrusts is 20°, a displacement of at least 2 km is estimated for the hanging wall of the Suzume fault to account for the observed 0.5 km thickness of the horses and the 0.5 km down-dip length of the flat-on-flat geometry of the thrust in the Okitsu duplex (Fig. 2c). Assuming that the footwalls of the Suzume fault was translated beneath the décollement from the trench before being underplated, as indicated by the modern Nankai subduction zone (Park et al., 2002a), at least 30 km of displacement is estimated for the footwall. Thus, the displacement across the Suzume fault, as well as expected deformation paths between the hanging wall and the footwall,

are dramatically different. The formation and displacement of the hanging wall along the thrust took place during underplating at the maximum burial depth of the mélange, which is thought to be the updip limit of seismogenesis (Matsumura et al., 2003). The footwall was deformed over a broad range of pressure-temperature (P-T) conditions throughout both underthrusting and underplating. At the prism toe in Nankai, a P-T condition of 20 MPa and 50 °C is measured at the upper part of the underthrust section in extremely porous sediments (porosity of 50%) and pillow basalts (porosity of 10%; Bourlange et al., 2003) where the region is thought to be aseismic (e.g. Hyndman et al., 1997). In contrast, sediments are expected to become progressively lithified up to the P-T conditions of underplating, and both basalt and sedimentary rocks in the Okitsu mélange have the porosity of less than 1% (Kato et al., 2004).

5.2. Comparison to décollement zones at prism toe regions

Three modern décollements have been penetrated by scientific ocean drilling in Barbados, Nankai, and Costa Rica (Moore and Klaus, 2000; Silver et al., 2001; Mikada et al., 2005; Morris et al., in press). The structure of the décollement zone, as defined by recovered cores and geophysical logs, consists of a tens-of-meters-thick zone of breccias and sub-horizontal fractures at the prism toes (Fig. 14a; Behrmann et al., 1988; Maltman et al, 1993; Vannucchi and Tobin, 2000). The brittle deformation appears at the top of the décollement zone, increases in intensity downwards, and then abruptly diminishes in the underthrust section (e.g. Morgan and Karig, 1995). No significant décollement-related ductile deformation or shear fabric is recognized at the core scale in the underthrust sediments in Barbados (Behrmann et al., 1988; Moore, 1989) and Nankai (Maltman et al., 1993; Ujiie et al., 2003). In contrast, the Costa Rica décollement zone is composed of 20-m-thick fractured zone in the upper part and 10-m-thick zone of ductile shear and folds in the lower part (Vannucchi and Tobin, 2000; Tobin et al., 2001). In addition, below the décollement zone there is a 180 m zone of non-coaxial shear that transitions downwards to layer-normal uniaxial shortening in the underthrust sediments at the Costa Rica site (Housen and Kanamatsu, 2003). In the toe regions, the

Fig. 14. Modified tectonic model of accretionary underthrusting and underplating displaying structural evolution of plate-boundary décollement on the basis of characterization of the Suzume fault, Okitsu mélange, and comparison to modern décollement zones drilled at the prism toes and exhumed out-of-sequence-thrusts (OOSTs). (a) At the prism toe, fracturing and brecciation occur in the hanging wall of the décollement zone (e.g. Maltman et al., 1993). Vertical, uniaxial shortening initiates in unconsolidated sediments of the underthrust section at Nankai (i; e.g. Ujiie et al., 2003), whereas the upper part of the underthrust section involves ductile, non-coaxial shear at Costa Rica (ii; Housen and Kanamatsu, 2003). (b) In the middle to later stages of underthrusting, at greater consolidation state, ductile, compactive deformation of sediments results in boudinage under axi-symmetric flattening followed by compactive faulting under superposition of flattening and simple shear. (c) At the depth of underplating, the plate-boundary décollement is extremely localized within decimeter-thick ultracataclasite, indicating continual localization of deformation associated with progressive consolidation of the underthrust sediments. Where the plate boundary décollement steps down into the lower section of the underthrust section, i.e., underplating via duplex development, fractures and breccias are produced during updip propagation of the décollement tip through basalt and sedimentary rock. Throughout the prism toe and deep underplating regions, the hanging wall of the décollement zone is characterized by intense fracturing under sub-horizontal contraction. (d) Large-displacement OOSTs from greater depth are characterized by crystal plastic deformation postdated by brittle deformation in the hanging wall, whereas the footwall only records deformation at shallow depth because of thrust transport oblique to the isotherm (Kondo et al., 2005). Note that (c) represents a schematic structure of the Suzume fault zone. (i) Undeformed basalt protolith, (ii) Fracture damage zone, (iii) Ultracataclasite layer including mesoscale prominent shear fracture surface (PFS), (iv) Ductile shear zone, and (v) Flattened sedimentary protolith.

Structural Evolution along Plate-Boundary Décollement

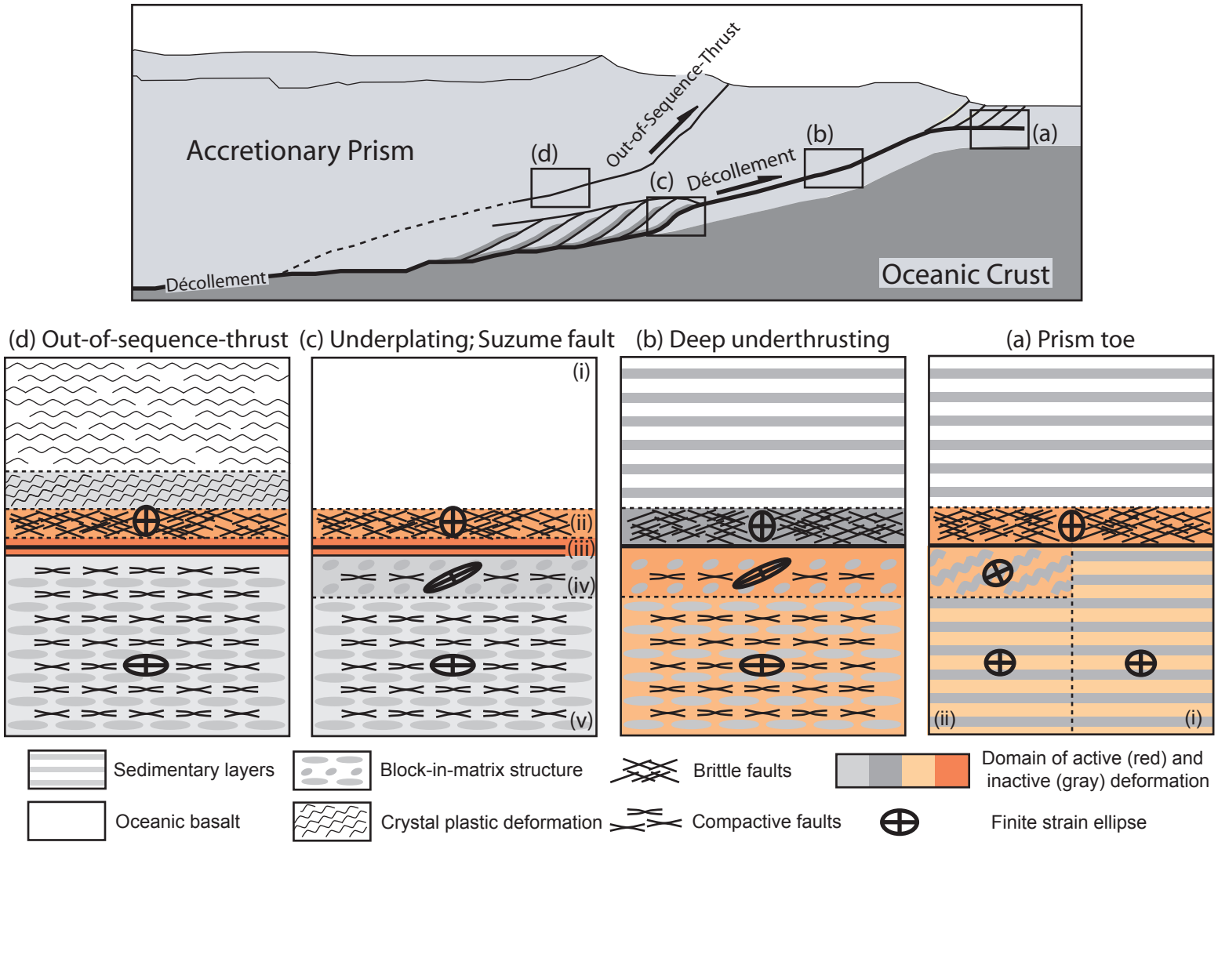

décollements constitute a discontinuity of stress-strain states between the accretionary prisms above and the underthrust sediments below. Sub-horizontal contraction dominates within the accretionary prisms, and sub-vertical contraction dominates in the underthrust sections (e.g. Moore, 1989; Karig and Morgan, 1994). Some of the characteristics of the décollements in the toe regions are also present in the Suzume fault of the Okitsu mélange, and comparison of the two settings provides some constraints on the evolution of the décollement zone during underthrusting and underplating.

The variation in styles of block-in-matrix structure present in the sedimentary section of the Okitsu mélange appears to record deformation during progressive consolidation of underthrust sediments, as suggested by others (e.g. Fisher and Byrne, 1987; Ujiie, 2002). For the flow-flow type, deformation of poorly consolidated sediments by particulate flow is suggested by disaggregated sand clasts in the shale between boudins and mud intrusion into the boudins (Fig. 8f; Ujiie, 2002). For the joint-flow type, sand layers were sufficiently lithified to maintain discrete fractures during deformation, whereas mineralization along fractures occurs at a certain P-T condition (Fig. 8b; Fisher and Byrne, 1987). These types of boudinage are consistent with early deformation of poorly consolidated material near the prism toe and later deformation of lithified sedimentary rocks at greater depth. The greater separation of boudins in the flow-flow and fault-flow types (Fig. 8b, f) suggests that the majority of stretch may have been established during the early stages of underthrusting than in the other types.

A strain path recorded in the block-in-matrix structure of the Okitsu mélange most likely involves axi-symmetric flattening normal to the sedimentary layering followed by minor non-coaxial shear, as suggested by Ujiie et al. (2000), because there is (1) uniform, very low magnitude stretch throughout the entire sedimentary section except in the vicinity of the Suzume fault (Fig. 13d), (2) similar magnitude of stretch inferred on slip-parallel and slip-perpendicular exposures and in sand layers cut by opposite verging shears in the fault-flow type (Fig. 8e), and (3) asymmetric boudinage only locally and a slight correlation between the thickness of sand layers and stretch, which could be

consistent with variable non-coaxial shear throughout the section with greater stretch in weaker layers.

Although the underthrust sections of modern prisms drilled to date do not display block-in-matrix structures, they do display a strain pattern similar to that in the Okitsu mélange (Fig. 14a). Magnetic fabrics indicate vertical, uniaxial shortening in the Nankai underthrust section reflecting overburden loading with significantly smaller horizontal stress (Ujiie et al., 2003). In contrast, non-coaxial strain is observed in the upper 180 m of the underthrust section in Costa Rica (Housen and Kanamatsu, 2003), probably because greater shear stress is transferred within the more consolidated sedimentary layers present in there than in the other regions due to better pore water drainage (Saffer, 2003). The Costa Rica case would lead to boudinage formation through localized shear with strain hardening along the master fault and downward diffusion of the sheared zone (Moore and Byrne, 1987), and resulting in large stretch with asymmetric boudinage in the upper most section of the underthrust sediments, a progressive decrease in stretch in the lower section (Fisher and Byrne, 1987), greater apparent stretch on slip-parallel than on slip-perpendicular exposures, a systematic development of asymmetric boudinage on slip-parallel exposures, and possibly strong correlation between stretch and lithology. The flattened sedimentary protolith of the Okitsu mélange shows little such features, but appear consistent with the strain state of the Nankai underthrust section. Nonetheless, because of the absence in the toe regions, the block-in-matrix structure likely formed during middle to later stages of underthrusting (Fig. 14b). Alternatively, the early types of boudinage may initiate in the toe region if the underthrust section consist of interbedded sandstone and shale similar to the sedimentary section of the Okitsu mélange.

A strain state inferred from the mesoscale faults in the sedimentary section of the Okitsu mélange is consistent with distributed, uniform flattening normal to the sedimentary layering and extension and minor simple shear parallel to the thrust transport direction of the Suzume fault, as evidenced by (1) distributed fractures throughout the footwall with no apparent increase in density near the Suzume fault

surface (Fig. 13f), (2) direction of shortening and extension indicated by the mesoscale faults (Fig. 12f) and the normal faults disrupting sedimentary strata at the outcrop (Fig. 8e), and (3) the existence and orientation of the point maxima of the fault B-axes (Fig. 12f). Taken together, the mesoscale faults must have occurred while sediments were only partially lithified because of (1) the extremely large dihedral angles of the conjugate faults (Fig. 8e; Wong et al., 2001) and (2) pronounced drag folding without fractures along the faults (Fig. 8c).

Compactive deformation bands that are at high angles from the maximum principal shortening stress have been observed in modern (e.g. Ujiie et al., 2004) and ancient (Byrne, 1984) accretionary prisms and other sedimentary basins (e.g. Shipton and Cowie, 2001) as well as in compaction experiments on porous sedimentary rocks (Wong et al., 2001). However, the orientation of the mesoscale faults nearly parallel to the sedimentary layering in the Okitsu mélange (Figs. 10b, 12a) is not compatible with the failure angles observed in laboratory experiments (Wong et al., 2001) and in outcrop scale conjugate faults in the mélange (Fig. 8e), and this may reflect significant rotation by subsequent layer-normal flattening.

Nonetheless, the mesoscale fault fabric is clearly related to the Suzume fault and most consistent with the later stages of non-coaxial shear inferred from the block-in-matrix structures resulted from. A similar orthorhombic fabric is observed in the underthrust sediments at Costa Rica (Housen and Kanamatsu, 2003), which appear to be more lithified than those in the other drilled margins (Saffer, 2003). By analogy, the compaction-related faults in the sedimentary rocks of the Okitsu mélange may have formed during middle to later stages of underthrusting in which shear stress at the décollement is transferred through more lithified sediments in the underthrust section (Fig. 14b).

The ductile shear zone in the footwall of the Suzume fault is somewhat similar to the lower part of the modern Costa Rica décollement zone that displays ductile shear, folds, swirled and mixed rock (Tobin et al., 2001) in more lithified sediments (Saffer, 2003). This analogy would imply that the ductile shear zone was initiated during early to

middle stages of underthrusting (Fig. 14b). Furthermore, the ductile shear zone of the Suzume fault appears to record greater shear associated with subsequent underthrusting to greater depth, as indicated by large stretch (Fig. 13d) and pronounced foliation (Fig. 9d). The localization of shear into the 20-m-thick zone may result from greater pore fluid pressures in the uppermost section of the underthrust sediments and smaller effective stresses in the ductile shear zone than in the rest of the section, or from an underconsolidated state in the zone that in turn leads to smaller strength of the zone (Bolton et al., 1998; Tobin et al., 2001).

The layer of dark gray ultracataclasite at the top of the footwall must have been a late stage feature of the Suzume fault which resulted, at least in part, from juxtaposition of the two host rocks, because (1) it and the grayish yellow green ultracataclasite forms the contact between the pillow basalt and the sedimentary rocks, (2) the PFS, along which at least some of the ultracataclasite was likely produced, truncates all other structures in the fault zone except for the high angle cross-faults, (3) a similar appearance in both ultracataclasite, as well as porphyroclasts of the grayish yellow green ultracataclasite included in the dark gray ultracataclasite layer, suggests that both ultracataclasites formed concurrently, and (4) ultracataclasite is a characteristic product of brittle faulting at several km depth in lithified rocks (e.g. Sibson, 1977). The lack of ultracataclasites in the modern décollement zones at the prism toes (Ujiie et al., 2003; Vannucchi and Tobin, 2000), along with the fact that the grayish yellow green ultracataclasite in the hanging wall must have formed only over the several km of displacement during underplating, implies that the dark gray ultracataclasites likely formed during underplating (Fig. 14c). At the given displacement, the decimeter-thick ultracataclasite layer of the Suzume fault is compatible with previous observation of scaling ultracataclasite layer thickness to displacement for brittle fault zones (Scholz et al., 1993; An and Sammis, 1994; Sibson, 2003).

As such, coexistence of ductile and brittle deformation in the footwall of the Suzume fault zone is consistent with the tectonic path of underthrust sediments from the prism toe to underplating regions. The sediments likely were consolidated via diagenesis,

metamorphism, and bulk compactive deformation, driven by increase in P-T conditions and long times. Consolidation could lead to a decrease in the ductility of sediments and thus promote brittle failure and localization of deformation (Fig. 14). The alternative hypothesis, that consolidation of sediments originates from localized shear and then deformation diffuse to surrounding weaker sediments from strain hardening, and then eventually accumulated in the entire section (Moore and Byrne, 1987), is not consistent with the timing relations in the Suzume fault.

It is also possible that the production of ultracataclasite by brittle processes may have been promoted by large strain rates during earthquake slips, whereas the ductile shear zone originated from small rate slips during the interseismic periods at greater depth. Experimental studies have demonstrated that flow by crystal plastic deformation mechanism could occur in shale at low to intermediate strain rates and the P-T condition of the maximum burial in the Okitsu mélange (Ibanez and Kronenberg, 1993). However, the ductile shear zone in the footwall of the Suzume fault shows little evidence of crystal plastic deformation, at least at the macroscopic scale.

The strain path inferred for the sedimentary section of the Okitsu mélange is dominated by large magnitude of shortening normal to the sedimentary layering with only small magnitude of layer-parallel extension during underthrusting from the prism toe to greater depth (Fig. 14). Whereas vertical, uniaxial shortening to axi-symmetric flattening occurs in the underthrust section at the prism toe, a transition to orthorhombic strain at greater depth from increased coupling across the plate boundary is expected on the basis of the correlation between diagenesis and frictional property of sediments (e.g. Moore and Saffer, 2001).

The mesoscale faults in the hanging wall must be related to the Suzume fault on the basis of fault density distribution (Fig. 11a, b) and fault fabrics and kinematics (Fig. 12e). The preferred orientation of the fault B-axes parallel to the thrust strike (Fig. 12b), and a contraction direction that is at a low angle to the Suzume fault surface inferred from the quasi-conjugate geometry (Fig. 12e) are consistent with the thrust kinematics. In the context of the tectonic model, the mesoscale faults and progressive intensification of

cataclasis inward towards an ultracataclasite layer record the formation of the décollement and the subsequent movement along the horse-bounding thrust to form the duplex (Fig. 14c).

The asymmetric structure of the Suzume fault clearly originated, at least in part, from the distinctly different lithology and dissimilar deformation history of the hanging wall and footwall. However, some aspects of the asymmetry, such as the difference in fracture fabric in the hanging wall and footwall, may reflect other factors. The observed fracture fabric is consistent with quasi static stress-states expected from mechanical analysis of accretionary wedges above a weak detachment (e.g. Hubbert and Rubey, 1959; Davis et al., 1983). However, the asymmetric fracture fabric in the Suzume fault could also arise for other reasons, such as from preferred propagation direction of repeated slip events along the boundary between two rocks with different mechanical properties (Ben-Zion and Shi, 2005). The mesoscale fault fabric in the hanging wall is consistent with the expected stress perturbation at the tip of a thrust that propagates updip. For updip propagation either during fault growth or associated with repeated earthquake ruptures (e.g. McGuire et al., 2002), shortening at low angles to the master fault is expected at the fault tip region in the hanging wall (e.g. Cowie and Scholz, 1992; Rice et al., 2005).

The deformation style and fabric in the cataclasite zone and fractured protolith of the hanging wall of the Suzume fault appears to be very similar to that in the hanging wall of all three of the modern décollement zones drilled at the prism toes (Behrmann et al., 1988; Vannucchi and Tobin, 2000; Ujiie et al., 2003). This similarity implies that such a feature is common for the hanging wall of the plate-boundary décollement throughout the prism toe to underplating regions (Fig. 14a, c).

5.3. Comparison to out-of-sequence-thrusts (OOSTs)

The structure of OOSTs varies with displacement. OOSTs with only hundreds of meters in displacement display a narrow, symmetric zone of brittle deformation (Mukoyoshi et al., 2006). In contrast, the Nobeoka thrust with displacement of 10 km

consists of a wide zone of fault-related crystal plastic deformation postdated by a narrow cataclastic zone in the hanging wall and a wide zone of brittle deformation with voluminous vein mineralization in the footwall (Fig. 14d; Kondo et al., 2005). Although the Suzume fault has several kilometers of displacement, the deformation is not consistent with that observed in the Nobeoka thrust.

OOSTs that occur in accretionary prisms are generally steeper than plate-boundary décollements as imaged in a modern subduction zone (Fig. 1a; Park et al., 2002b). At the km scale, the majority of transport would be horizontal in plate-boundary décollements, whereas significant vertical transport occurs accounted for a given displacement in OOSTs. Accordingly, a higher paleo temperature is expected to be recorded in hanging walls than footwalls in OOSTs due to movement oblique to isotherms. In fact, paleo temperature offsets are used to identify OOSTs in exhumed, ancient accretionary prisms (Ohmori et al., 1997; Kondo et al., 2005; Mukoyoshi et al., 2006). Fault related processes, such as fluid flow and mass transportation, may be enhanced by the depth contrast between the two ends of fault in OOSTs. For instance, voluminous precipitation of vein minerals, and possibly dis-equilibrium in paleo temperature between veins along faults and host rocks may be expected (Kondo et al, 2005).

No gap in paleo temperature across the Suzume fault is indicated by illite crystallinity analysis (Sakaguchi and Takami, pers. comm.), which is consistent with the fault being a segment of a fossilized décollement without significant reactivation as an OOST during exhumation. Both the hanging wall basalts and footwall sedimentary rocks must have reached approximately the same, maximum burial depth, because both were carried together by the subducting slab, which resulted in no gap in paleo temperature structure between the hanging wall and the footwall.

The relation of structures compatible with modern décollement zones at the prism toe regions, as well as the lack of structures characteristic of OOSTs, suggest that the Suzume fault was not significantly reactivated as an OOST and preserves deformation related to the plate-boundary décollement without significant subsequent deformation,

except for minor, high-angle cross faults associated with exhumation. Uplift of the Okitsu mélange as a relatively rigid body along nearby OOSTs is consistent with the rapid uplifting indicated by the extreme short time span between sedimentation in 74 MA and the cooling age for 200 °C of 70 MA (Fig. 3). Possible OOSTs are the tectonic boundaries of the Okitsu mélange with the surrounding formations (Ikesawa et al., 2003) or the faults in the Shimanto belt that offset paleo-thermal structure (Ohmori et al., 1997; Mukoyoshi et al., 2006). Alternatively, relatively slow uplifting, indicated by the 60 million years between the cooling ages of 200 °C and 100 °C (Hasebe et al., 1993; Tagami et al., 1995), may have been accommodated simply by compensating surface erosion (e.g., Davis et al., 1983) with relatively insignificant deformation associated with uplifting.

6. DISTRIBUTION OF SHEAR AND FAILURE MODE IN THE ULTRACATACLASITE LAYER

Shear displacement in the hanging wall of the Suzume fault appears to be accommodated largely in the ultracataclasite layer and only partly in the cataclasite zone that includes the tabular porphyroclasts and the parallel faults (Fig. 11b, d). In the footwall, both the ductile shear zone and the dark gray ultracataclasite layer likely accommodate significant shear displacement. Structural relations are consistent with extreme localization of shear to the PFS within the ultracataclasite layer (Figs. 5, 6), similar to inferences from the structure of other fault zones (e.g. Chester and Chester, 1998; Tanaka et al, 2001; Sibson, 2003; Heermance et al., 2003). Although the abrupt change in particle size from the cataclasites to the ultracataclasite is taken as evidence for extreme localization of slip to the ultracataclasite, the ultracataclasites of the Suzume fault contain a significant volume of mesoscopic porphyroclasts of host rock lithologies relative to other large-displacement faults that display uniform, very-fine grain size (e.g. Chester et al., 1993; 2005; Ohtani et al., 2000). This could reflect a difference in displacement and the degree of localization between faults, or a difference in the rate of comminution of the different lithologies that make up the host rocks (Jackson and Dunn, 1974).

Mesoscale faulting may have been the main brecciation process, compatible with crush brecciation noted by Sibson (1986), in the outer cataclasite zone of the hanging wall because the decrease in pillow clast size towards the ultracataclasite layer correlates with the increase in the parallel fault density and change in clast shape from equi-dimensional to tabular. In the inner cataclasite zone and in both ultracataclasites, attrition brecciation (Sibson, 1986) may have been predominant, inferred from a large amount of shear and the porphyroclasts composed of older matrix and porphyroclasts that record repeated slips, as expected by Sibson (1986). Change in clast shape indicates that the tabular porphyroclasts in the ultracataclasite layer could have been ripped off from the surrounding cataclasite zone and incorporated in the layer, similar to that noted by Swanson (1989).

Although there are profound differences in the structure of rock surrounding the ultracataclasite layers in the Suzume fault and Punchbowl fault as described by Chester and Chester (1998), the structure and inferred evolution of the ultracataclasite appears very similar. On the basis of structural criteria similar to that used by Chester and Chester (1998), the grayish yellow green ultracataclasite and the dark gray ultracataclasite are interpreted to be derived from the pillow basalt and the sedimentary rocks, respectively. For the grayish yellow green ultracataclasite and basalt, (1) the color of the ultracataclasite is similar to the host rock, (2) most of the basalt porphyroclasts are contained in the grayish yellow green ultracataclasite, (3) clast size and abundance decreases towards the contact with the other ultracataclasite, and (4) one side of the grayish yellow green ultracataclasite is always next to the surrounding deformed basalt (Figs. 5, 6). A similar spatial relationship is observed between the dark gray ultracataclasite and the sedimentary rocks.

The mapped structure suggests that the formation of each ultracataclasite may have started within each corresponding rock, and then the two ultracataclasites were placed into direct contact by localized slip as the two host rocks were juxtaposed by large displacement, similar to that proposed for the Punchbowl fault by Chester and Chester (1998). The PFS must have been operative during the last stage of the Suzume fault history, because (1) most internal fabric and fractures are cut by the PFS, and (2) there is a less-cohesive, presumably most recently reworked ultracataclasite layer adjacent to the PFS.

Faults bearing ultracataclasite layers derived from both (e.g. Chester and Chester, 1998) or either (e.g. Cowan et al., 2003; Wibberley and Shimamoto, 2003) of two host rock types have been documented. Assuming localized slip as the failure mode, and that the ultracataclasite is produced by attrition wear (Sibson, 1986), the generation of new ultracataclasite from one host rock would require the slip surface to be located at the boundary of host rock and ultracataclasite layer or within the host rock. Presence of the slip surface within the ultracataclasite would lead to reworking and mixing of ultracataclasite types (Chester et al., 2004). In the Suzume fault, the formation of

grayish yellow green ultracataclasite by localized slip and wear is consistent with somewhat more uniform and finer clast size and greater volume than that of the dark gray ultracataclasite layer, and that 80% of the PFS is located either at the boundary between the basalt and the grayish yellow green ultracataclasite or within the grayish yellow green ultracataclasite (Table 1). The localization of the PFS suggests during the final stages of displacement the slip was concentrated in the ultracataclasite and hanging wall cataclasite.

These overall spatial relations, as well as little evidence for mixing of ultracataclasites or stacking of fault bounded slices of the two ultracataclasites, suggest that the localized slip on the PFS must have been maintained in the ultracataclasite layer at least for the time after the basalt and sedimentary rocks were juxtaposed, similar to relations documented in other faults (e.g. Chester and Chester, 1998; Tanaka et al, 2001; Sibson, 2003). However, minor mixing did occur repeatedly, at least during later stages of deformation, because (1) the PFS branches locally and truncates the ultracataclasite contact, and (2) the porphyroclasts, slivers, and patches of the ultracataclasite may represent the remnants of past branching and mixing across the ultracataclasite contact.

The structure of the ultracataclasite contacts records both flow and localized slip as the mesoscale mode of failure. Flow of ultracataclasites likely occurred, as evidenced by the undulatory, interfingering contact of the two ultracataclasites and mesoscale injection of the ultracataclasites into fractures (e.g. Lin, 1996; Otsuki, 2005), as well as the presence of patches of grayish yellow green ultracataclasite in the dark gray ultracataclasite layer, possibly. In the mapped region the ultracataclasite injection is a relatively minor feature, and there is little fabric indicative of flow, such as vortex and flame textures. Repeated slip along localized surfaces is suggested by the possible presence of past PFS along basalt porphyroclasts with discrete edges present within the ultracataclasite layer. Although the majority of the ultracataclasite contact structure indicates flow and is not consistent with localized slip as its origin (Figs. 5, 6), the coexistence of structures indicative of localized slip and distributed flow may be associated with the seismic cycling of fast- and slow-rate slips (e.g. Sibson, 1989;

Tanaka et al., 2001). The extreme localization of slip may correlate with rate-weakening behavior and unstable slip during the coseismic period of the seismic cycle (Chester and Chester, 1998; Sibson, 2003). Distributed flow via, for instance, creep compaction by pressure solution and slow crack growth, is thought to be operative during interseismic periods (Sibson, 1989; Chester et al., 1993).

7. COMPARISON TO STRUCTURE OF OTHER LARGE-DISPLACEMENT, BRITTLE FAULTS

The complex structure of the footwall of the Suzume fault must reflect change in the mode of deformation due to large displacement and vertical transport, i.e., depth of burial. The 30 km of translation must have led to change in P-T conditions that also would have contributed to change in host rock properties, such as porosity, strength, and ductility of the sedimentary rock, over the history of the fault (e.g. Moore and Saffer, 2001). The ductile shear zone and flattened protolith likely resulted from compactive, ductile deformation of poorly consolidated sediments in the aseismic regime, as similar compactive deformation is observed in modern (e.g. Maltman et al., 1993) and ancient (e.g. Byrne, 1984; Fisher and Byrne, 1987) accretionary prisms, whereas the generation of dark gray ultracataclasite layer would be consistent with the brittle, localized shear of lithified sedimentary rocks at the seismogenic regime. Dip-slip fault zones recording varied P-T regimes have been documented, in particular those composed of crystal plastic deformation at the quasi-plastic regime followed by localized, brittle deformation at the seismogenic regime (e.g. Sibson, 1977; Kondo et al., 2005). At a low P-T condition, a narrow gouge zone bounded by a zone of ductile shear, disrupted strata, folds, and compactive deformation (Lohr et al., 1999; Rawling et al., 2001) may reflect change in host rock properties, transitioning from distributed shear in poorly consolidated sediments to localized shear in more consolidated sedimentary rocks.

In contrast, the relatively simple structure of the hanging wall of the Suzume fault likely reflects deformation at a single P-T condition, consistent with the inferred P-T-d-t history of the Okitsu mélange and underplating at the maximum burial depth over a geologically short time span (Hasebe et al., 1993; Tagami et al., 1995; Sakaguchi, 1996; Matsumura et al., 2003). This is similar to relatively uniform deformation modes that may be expected for transform plate boundary faults in crystalline rocks with displacements at a relatively constant depth where evolution in host rock properties is minimized (e.g. Chester et al., 1993; Ohtani et al., 2000). In these cases an increase in displacement would contribute to the intensification of fabric development and

homogenization of fault zone properties along the strike of faults (Shipton and Cowie, 2001). In ancient traces of San Andreas fault system with tens of kilometers displacement, subsidiary fractures display a distinct increase in density across the fault, and the development of fabrics are similar along the strike of the fault (e.g. Chester et al., 1993). Also, the uniform, ultra-fine-grained ultracataclasites may have resulted from the repeated reworking during numerous slip events as large displacements were achieved (e.g., Chester and Chester, 1998; Ohtani et al., 2000). Intensification of fault zone fabrics is expected to be less in the Suzume fault because the displacement of the hanging wall is limited to several kilometers. Although likely faulted at a single P-T condition, the hanging wall displays significantly less increase and more heterogeneity in fracture density along and across the fault than seen in transform faults with tens of kilometers in displacement, such as the Punchbowl fault (e.g., Chester et al., 1993) and the Nojima fault (Lin et al., 2001).

Geometric relations between fault planes and host rock layering may also affect on fault structure development. Off-fault, subsidiary deformation, such as secondary fractures, is necessary for new fracture development and growth (e.g. Cowie and Scholz, 1992; Lockner et al., 1992). However, fault formation along pre-existing weak planes, such as sedimentary layering, may produce much less subsidiary deformation than in mechanically isotropic rocks (e.g., Scholz, 1993). The relatively focused brittle deformation in the hanging wall of the Suzume fault may be attributed to fault development along pre-existing, weak stratigraphic horizons as evidenced by the flat-on-flat geometry. Similarly, the northern Chelugpu fault also displays a flat-on-flat geometry and appears to display a narrower fault zone than the southern Chelugpu fault consisting of a flat-on-ramp (Heermance et al., 2003). In contrast, for transform settings, faulting often occurs in mechanically isotropic host rocks or oblique to weak plane configurations (e.g., Chester et al., 1993; Ohtani et al., 2000), which may have resulted in broader fault zones.

The hanging wall of the Suzume fault would fit the simple damage zone and fault core structural model from observations of large-displacement, strike-slip faults in

crystalline rocks (e.g. Chester et al., 1993; Caine et al., 1996). The fractured protolith and zones of foliated cataclasite and ultracataclasite would constitute the damage zone and fault core, respectively. However, modification of the model is required to describe the entire fault zone structure. The ductile shear zone of the footwall is somewhat similar to the mixed zone of the Sand Hill fault (Rawling et al., 2001) and the ductile shear zone in the modern Costa Rica décollement zone (Tobin et al., 2001) which record distributed shear in poorly consolidated sediments. Both ductile shear zone and dark gray ultracataclasite layer could be regarded as the fault core of the footwall (Fig. 7) because of the accommodation of large shear displacement and destruction of the original sedimentary structure (Chester et al., 1993).

8. CONCLUSION

In the Suzume fault of the Okitsu mélange, pillow basalt of the hanging wall is characterized by a decimeter-thick layer of ultracataclasite, bounded by a several-meter-thick zone of cataclasite, which progressively transitions with distance through a fractured zone to the relatively undeformed host rock. Sedimentary rocks of the footwall display a decimeter-thick layer of ultracataclasite bounded by a 20-meter-thick zone of ductile shear, which transitions to the flattened sedimentary host rock marked by pervasive block-in-matrix structure. Inferred strain state is consistent with contraction at low angles to the Suzume fault surface in the hanging wall and flattening normal to the surface in the footwall.

The deformation style and fabric in the cataclasite zone of the hanging wall in the Suzume fault is consistent with that observed in the hanging wall of the décollement zones at the toe region of modern accretionary prisms, implying such features are common in the hanging wall of the décollement zone at the toe and underplating regions. The strain state inferred for the ductile shear zone and flattened sedimentary protolith in the footwall of the Suzume fault is consistent with that inferred for the modern Costa Rica underthrust sediments. Hence, the two zones of the Suzume fault resulted from compactive deformation of unconsolidated sediments during underthrusting from shallow to greater depths. At the depth of underplating, shear displacement along the décollement zone appears to be extremely localized into decimeter-thick ultracataclasite which is a characteristic deformation mode of seismic faults in crystalline and lithified sedimentary rock at depth. Accordingly, the three zones of the footwall in the Suzume fault likely reflect progressive localization of deformation, associated with progressive consolidation of the underthrust sediments. Thus, the asymmetric structure of the Suzume fault is consistent with the tectonic model of the plate-boundary décollement where the footwall records deformation associated with both underthrusting and underplating, and the hanging wall only reflects deformation associated with underplating at the latest stages of the fault history.

Structure of the ultracataclasite layer derived from the two host rock types, which represents the macroscopic Suzume fault surface, is consistent with alternating, cyclic failure of the layer by extremely localized slip and distributed shearing flow.

Structure of the hanging wall in the Suzume fault zone would fit the damage zone and fault core model, whereas the footwall is consistent with the model, as modified by Rawling et al. (2001), by addition of mixing zone to account for ductile deformation in poorly consolidated materials.

REFERENCES

An, L. J., Sammis, C. G. 1994. Particle-size distribution of cataclastic fault materials from Southern California - A 3-D study. Pure and Applied Geophysics 143(1-3), 203-227.

Behrmann, J. H., Brown, K., Moore, J.C., Mascle, A., Taylor, E., Alvarez, F., Andreieff, P., Barnes, R., Beck, C.J., Blanc, G., Clark, M., Dolan, J., Fisher, A., Gieskes, J., Hounslow, M., McLellan, P., Moran, K., Ogawa, Y., Sakai, T., Schoonmaker, J., Vrolijk, P., Wilkens, R., Williams, C. 1988. Evolution of structures and fabrics in the Barbados Accretionary Prism. In: Insights from Leg 110 of the Ocean Drilling Project. Journal of Structural Geology 10(6), 577-591.

Ben-Zion, Y., Sammis, C. G. 2003. Characterization of fault zones. Pure and Applied Geophysics 160(3-4), 677 - 715.

Ben-Zion, Y., Shi, Z. 2005. Dynamic rupture on a material interface with spontaneous generation of plastic strain in the bulk. Earth and Planetary Science Letters 236(1-2), 486-496.

Berg, S. S., Skar, T. 2005. Controls on damage zone asymmetry of a normal fault zone: Outcrop analyses of a segment of the Moab fault, SE Utah. Journal of Structural Geology 27(10), 1803-1822.

Bolton, A. J., Maltman, A.J., Clennell, M.B. 1998. The importance of overpressure timing and permeability evolution in fine-grained sediments undergoing shear. Journal of Structural Geology 20(8), 1013-1022.

Bourlange, S., Henry, P., Moore, J. C., Mikada, H., Klaus, A. 2003. Fracture porosity in the décollement zone of Nankai accretionary wedge using logging while drilling resistivity data. Earth and Planetary Science Letters 209(1-2), 103-112.

Bruhn, R. L., Parry, W. T., Yonkee, W. A., Thompson, T. 1994. Fracturing and hydrothermal alteration in normal fault zones. Pure and Applied Geophysics 142(3/4), 609-644.

Byrne, T. 1984. Early deformation in melange terranes of the Ghost Rocks Formation, Kodiak Islands, Alaska. In: Raymond, L.A. (Eds.), Melanges: Their Nature, Origin and Significance. Geological Society of America Special Paper 198, 21-52.

Caine, J. S., Evans, J.P., Forster, C.B. 1996. Fault zone architecture and permeability structure. Geology 24(11), 1025-1028.

Chester, F. M., Logan, J. M. 1986. Implications for mechanical properties of brittle faults from observations of the Punchbowl fault zone, California. Pure and Applied Geophysics 124(1-2), 79-106.

Chester, F. M., Evans, J.P., Biegel, R.L. 1993. Internal structure and weakening mechanisms of the San Andreas fault. Journal of Geophysical Research 98(B1), 771-786.

Chester, F. M., Chester, J.S. 1998. Ultracataclasite structure and friction processes of the Punchbowl fault, San Andreas system, California. Tectonophysics 295(1-2), 199-221.

Chester, F. M., Chester, J.S., Kirschner, D.L., Schulz, S.E., Evans, J.P. 2004. Structure of large-displacement strike-slip fault zones in the brittle continental crust. In: Karner, G.D., Taylor, B., Driscoll, N.W., Kohlstedt, D.L. (Eds.), Rheology and Deformation in the Lithosphere at Continental Margins, MARGINS Theoretical and Experimental Earth Science Series 1, Columbia University Press, New York, 223-260.

Chester, J. S., Chester, F. M., Kronenberg, A.K. 2005. Fracture surface energy of the Punchbowl fault, San Andreas system. Nature 437(7055), 133-136.

Cowan, D. S., Cladouhos, T. T., Morgan, J. K. 2003. Structural geology and kinematic history of rocks formed along low-angle normal faults, Death Valley, California. Geological Society of America Bulletin 115(10), 1230-1248.

Cowie, P. A., Scholz, C.H. 1992. Physical explanation for the displacement-length relationship of faults using a post-yield fracture mechanics model. Journal of Structural Geology 14(10), 1133-1148.

Davis, D., Suppe, J. and Dahlen, F.A. 1983. Mechanics of fold-and-thrust belts and accretionary wedges. Journal of Geophysical Research 88(B2), 1153–1172.

Evans, J. P., Chester, F.M. 1995. Fluid-rock interaction in faults of the San Andreas system: Inferences from San Gabriel fault rock geochemistry and microstructures. Journal of Geophysical Research 100(B7), 13,007–13,020.

Evans, J. P., Forster, C.B., Goddard, J.V. 1997. Permeability of fault-related rocks, and implications for hydraulic structure of fault zones. Journal of Structural Geology 19(11), 1393-1404.

Faulkner, D. R., Lewis, A.C., Rutter, E.H. 2003. On the internal structure and mechanics of large strike-slip fault zone: Field observations of the Carboneras fault in southeastern Spain. Tectonophysics 367(3-4), 235-251.

Fisher, D., Byrne, T. 1987. Structural evolution of underthrusted sediments, Kodiak Islands, Alaska. Tectonics 6(6), 775-793.

Gettemy, G. L., Tobin, H.J., Hole, J.A., Sayed, A.Y. 2004. Multi-scale compressional wave velocity structure of the San Gregorio Fault zone. Geophysical Research Letters 31(L06601), doi:10.1029/2003GL018826.

Goldstein, A., Marshak, S. 1988. Analysis of fracture array geometry. In: Marshak, S., Mitra, G. Basic Methods of Structural Analysis, Prentice-Hall, Englewood Cliffs, New Jersey, 249-268.

Goscombe, B. D., Passchier, C.W., Hand, M. 2004. Boudinage classification: End-member boudin types and modified boudin structures. Journal of Structural Geology 26(4), 739-763.

Hancock, P. L. 1985. Brittle microtectonics: Principles and practice. Journal of Structural Geology 7(3-4), 437-457.

Hasebe, N., Tagami, T., Nishimura, S. 1993. Evolution of the Shimanto accretionary complex: A fission-track thermochronologic study. Geological Society of America Special Paper 273, 121-36.

Hashimoto, Y., Kimura, G. 1999. Underplating process from melange formation to duplexing: Example from the Cretaceous Shimanto Belt, Kii Peninsula, southwest Japan. Tectonics 18(1), 92 - 107.

Heermance, R., Shipton, Z. K., Evans, J. P. 2003. Fault structure control on fault slip and ground motion during the 1999 rupture of the Chelungpu fault, Taiwan. Bulletin of the Seismological Society of America 93(3), 1034-1050.

Hickman, S. H. 1991. Stress in the lithosphere and the strength of active faults. Review of Geophysics 29(S), 759–775.

Housen, B. A., Kanamatsu, T. 2003. Magnetic fabrics from the Costa Rica margin: Sediment deformation during the initial dewatering and underplating process. Earth and Planetary Science Letters 206(1-2), 215-228.

Hubbert, M. K., Rubey, W. W. 1959. Role of fluid pressure in mechanics of overthrust faulting. Geological Society of America Bulletin 70(2), 115-166.

Hyndman, R. D., Yamano, M., Oleskevich, D.A. 1997. The seismogenic zone of subduction thrust faults. The Island Arc 6(3), 244.

Ibanez, W. D., Kronenberg, A.K. 1993. Experimental deformation of shale: Mechanical properties and microstructural indicators of mechanisms. International Journal of Rock Mechanics and Mining Science & Geomechanics 30(7), 723-734.

Ikesawa, E., Sakaguchi, A., Kimura. G. 2003. Pseudotachylyte from an ancient accretionary complex: Evidence for melt generation during seismic slip along a master décollement? Geology 31(7), 637-640.

Jackson, R. E., Dunn, D.E. 1974. Experimental sliding friction and cataclasis of foliated rocks. International Journal of Rock Mechanics and Mining Sciences 11(6), 235-249.

Kanaya, T. 2001. Detailed internal structure of Okitsu melange, Shimanto belt, southwest Japan (in Japanese with English abstract). B.S. Thesis, Kochi University.

Kanaya, T., Sakaguchi, A. 2006. Structure of Okitsu melange, Shimanto accretionary complex, Japan (unpublished manuscript). Department of Geology, Kochi University.

Karig, D. E., Morgan, J.K. 1994. Tectonic deformation; stress paths and strain histories. In: A. Maltman (Eds.), The Geological Deformation of Sediments, Chapman and Hall, London, 167-204.

Kato, A., Sakaguchi, A., Yoshida, S., Yamaguchi, H., Kaneda, Y. 2004. Permeability structure around an ancient exhumed subduction-zone fault. Geophysical Research Letters 31(L06602), doi:10.1029/2003GL019183.

Kimura, G., Mukai, A. 1991. Underplated units in an accretionary complex: Melange of the Shimanto belt of eastern Shikoku, southwest Japan. Tectonics 10(1), 31 - 50.

Kondo, H., Kimura, G., Masago, H., Ohmori-Ikehara, K., Kitamura, Y., Ikesawa, E., Sakaguchi, A., Yamaguchi, A., Okamoto, S. 2005. Deformation and fluid flow of a major out-of-sequence thrust located at seismogenic depth in an accretionary complex: Nobeoka Thrust in the Shimanto Belt, Kyushu, Japan. Tectonics 24, TC6008.

Lin, A. 1996. Injected veins of crushing-originated pseudotachylite and fault gouge formed during seismic faulting. Engineering Geology 43(2-3), 213-224.

Lin, A., Shimamoto, T., Maruyama, T., Sigetomi, M., Miyata, T., Takemura, K., Tanaka, H., Uda, S., Murata, A. 2001. Comparative study of cataclastic rocks from a drill core and outcrops of the Nojima Fault zone on Awaji Island, Japan. The Island Arc 10(3-4), 368-380.

Lockner, D. A., Byerlee, J.D., Kuksenko, V.S. 1992. Observations of quasistatic fault growth from acoustic emissions. In: Evans, B., Wong, T.-F. (Eds.), Fault Mechanics and Transport Properties of Rocks, Academic Press, London, 3-31.

Lohr, M., Yamagata, T., Moore, J.C. 1999. Structural fabrics and hydrocarbon content of the San Gregorio Fault zone, Moss Beach, California. In: Garrison, R.E., Aiello, I., Moore, J.C. (Eds.), Late Cenozoic Fluid Seeps and Tectonics along the San Gregorio Fault Zone in the Monterey Bay Region, California, American Association of Petroleum Geologists, Pacific Section, Bakersfield, CA GB-76, 21-34.

Maltman, A. J., Byrne, T., Karig, D.E., Lallemant, S. 1993. Deformation at the toe of an active accretionary prism: Synopsis of results from ODP Leg 131, Nankai, SW Japan. Journal of Structural Geology 15(8), 949-964.

Mandal, N., Chakraborty, C., Samanta, S. K. 2000. Boudinage in multilayered rocks under layer-normal compression: A theoretical analysis. Journal of Structural Geology 22(3), 373-382.

Matsumura, M., Hashimoto, Y., Kimura, G., Ohmori-Ikehara, K., Enjohji, M., Ikesawa, E. 2003. Depth of oceanic-crust underplating in a subduction zone: Inferences from fluid-inclusion analyses of crack-seal veins. Geology 31(11), 1005-1008.

McGuire, J. J., Zhao, L., Jordan, T.H. 2002. Predominance of unilateral rupture for a global catalog of large earthquakes. Bulletin of the Seismological Society of America 92(8), 3309-3317.

Mikada, H., Moore, G.F., Taira, A., Becker, K., Moore, J.C., and Klaus, A. 2005. Proceedings of the Ocean Drilling Program, Scientific Results, 190/196 [CD-ROM]. Available from: Ocean Drilling Program, Texas A&M University, College Station TX.

Miyashiro, A. 1973. Metamorphism and Metamorphic Belts. John Wiley & Sons, New York.

Moore, J. C. 1989. Tectonics and hydrogeology of accretionary prisms: Role of the décollement zone. Journal of Structural Geology 11(1-2), 95-106.

Moore, J. C., Byrne, T. 1987. Thickening of fault zones: A mechanism of mélange formation in accreting sediments. Geology 15(11), 1040-1043.

Moore, J. C., Klaus, A. 2000. Proceedings of the Ocean Drilling Program, Scientific Results, 171A [CD-ROM]. Available from: Ocean Drilling Program, Texas A&M University, College Station TX.

Moore, J. C., Saffer, D. 2001. Updip limit of the seismogenic zone beneath the accretionary prism of southwest Japan: An effect of diagenetic to low-grade metamorphic processes and increasing effective stress. Geology 29(2), 183-186.

Morgan, J. K., Karig, D.E. 1995. Décollement processes at the Nankai accretionary margin, southeast Japan: Propagation, deformation, and dewatering. Journal of Geophysical Research 100(B8), 15,221-15,232.

Morley, C. K. 1988. Out-of-sequence thrusts. Tectonics 7(3), 539-561.

Morris, J. M., Villinger, H.W., Klaus, A. in press. Proceedings of the Ocean Drilling Program, Scientific Results, 205 [CD-ROM]. Available from: Ocean Drilling Program, Texas A&M University, College Station TX.

Mukoyoshi, H., Sakaguchi, A., Otsuki, K., Hirono, T., Soh, W. 2006. Co-seismic frictional melting along an out-of-sequence thrust in the Shimanto accretionary complex. Implications on the tsunamigenic potential of splay faults in modern subduction zones. Earth and Planetary Science Letters 245(1-2), 330-343.

Needham, D. T. 1995. Mechanisms of mélange formation: Examples from SW Japan and southern Scotland. Journal of Structural Geology 17(7), 971-985.

Ohmori, K., Taira, A., Tokuyama, H., Sakaguchi, A., Okamura, M., Aihara, A. 1997. Paleothermal structure of the Shimanto accretionary prism, Shikoku, Japan: Role of an out-of-sequence thrust. Geology 25(4), 327-330.

Ohtani, T., K. Fujimoto, H. Ito, H. Tanaka, N. Tomida, T. Higuchi. 2000. Fault rocks and past to recent fluid characteristics from the borehole survey of the Nojima fault ruptured in the 1995 Kobe earthquake, southwest Japan. Journal of Geophysical Research 105(B7), 16161-16172.

Otsuki, K., Uduki, T., Monzawa, N., Tanaka, H. 2005. Clayey injection veins and pseudotachylyte from two boreholes penetrating the Chelungpu Fault, Taiwan: Their implications for the contrastive seismic slip behaviors during the 1999 Chi-Chi earthquake. The Island Arc 14(1), 22-36.

Park, J., Tsuru, T., Takahashi, N., Hori, T., Kodaira, S., Nakanishi, R. Miura, S., Kaneda, Y. 2002a. A deep strong reflector in the Nankai accretionary wedge from multichannel seismic data: Implications for underplating and interseismic shear stress release. Journal of Geophysical Research 107(B4), 2061-2072. doi:10.1029/2001JB000262.

Park, J. O., Tsuru, T., Kodaira, S., Cummins, P.R., Kaneda, Y. 2002b. Splay fault branching along the Nankai subduction zone. Science 297(5584), 1157-1160.

Passchier, C. W., Simpson, C. 1986. Porphyroclast systems as kinematic indicators. Journal of Structural Geology 8(8), 831-843.

Platt, J. P., Leggett, J.K., Young, J., Raza, H., Alam, S. 1985. Large-scale sediment underplating in the Makran accretionary prism, southwest Pakistan. Geology 13(7), 507-511.

Ramberg, H. 1955. Natural and experimental boudinage and pinch-and swell structures. Journal of Geology 63(6), 512-526.

Ramsay, J. G. 1967. Folding and Fracturing of Rocks. McGraw-Hill, New York.

Rawling, G. C., Goodwin, L. B., Wilson, J. L. 2001. Internal architecture, permeability structure, and hydrologic significance of contrasting fault-zone types. Geology 29(1), 43-46.

Rice, J. R. 1992. Fault stress states, pore pressure distributions, and the weakness of the San Andreas fault. In: Evans, B., Wong, T.F. (Eds.), Fault Mechanics and Transport Properties in Rocks. Academic Press, London, 475–503.

Rice, J. R., Sammis, C.G, Parsons, R. 2005. Off-fault secondary failure induced by a dynamic slip pulse. Bulletin of the Seismological Society of America 95(1), 109-134.

Saffer, D. M. 2003. Pore pressure development and progressive dewatering in underthrust sediments at the Costa Rican subduction margin: Comparison with northern Barbados and Nankai. Journal of Geophysical Research 108(B5), 2261-2276. doi:10.1029/2002JB001787.

Sakaguchi, A. 1996. High paleogeothermal gradient with ridge subduction beneath the Cretaceous Shimanto accretionary prism, southwest Japan. Geology 24(9), 795-798.

Scholz, C. H. 1990. The Mechanics of Earthquakes and Faulting. Cambridge University Press, Cambridge.

Scholz, C. H., Dawers, N.H., Yu,J.-Z., Anders, M.H., Cowie, P.A. 1993. Fault growth and fault scaling laws: Preliminary results. Journal of Geophysical Research 98(B12), 21951-21962.

Screaton, E. J., Wuthrich, D.R., Dress, S.J. 1990. Permeabilities, fluid pressures, and flow rates in the Barbados Ridge Complex. Journal of Geophysical Research 95(B6), 8997-9007.

Shipton, Z. K., Cowie, P.A. 2001. Shipton and Cowie, Damage zone and slip-surface evolution over μm to km scales in high-porosity Navajo sandstone, Utah. Journal of Structural Geology 23(12), 1825-1844.

Sibson, R. H. 1977. Fault rocks and fault mechanisms. Journal of the Geological Society of London 133(3), 191-213.

Sibson, R. H. 1986. Brecciation processes in fault zones: Inferences from earthquake rupturing. Pure and Applied Geophysics 124(1-2), 159-175.

Sibson, R. H. 1989. Earthquake faulting as a structural process. Journal of Structural Geology 11(1-2), 1-14.

Sibson, R. H. 2003. Thickness of the Seismic Slip Zone. Bulletin of the Seismological Society of America 93(3), 1169-1178.

Silver, E. A., Kimura, G., Blum, P., Shipley, T.H. 2001. Proceedings of the Ocean Drilling Program, Scientific Results, 170 [CD-ROM]. Available from: Ocean Drilling Program, Texas A&M University, College Station TX.

Snoke, A. W., Tullis, J. 1998. An Overview of Fault Rocks. In: Snoke, A.W., Tullis, J., Todd, V.R., (Eds.), Fault-Related Rocks. A Photographic Atlas. Princeton University Press, Princeton, New Jersey, 3-13.

Swanson, M. T. 1989. Sidewall ripouts in strike-slip faults. Journal of Structural Geology 11(8), 933-948.

Tagami, T., Hasebe, N., Shimada, C. 1995. Episodic exhumation of accretionary complexes: Fission-track thermochronologic evidence from the Shimanto Belt and its vicinities, southwest Japan. The Island Arc 4(3), 209-30.

Taira, A., Hill, I., Firth, J. 1991. Proceedings of the Ocean Drilling Program, Initial Reports, 131. Available from: Ocean Drilling Program, Texas A&M University, College Station TX.

Taira, A., Katto, J., Tashiro, M., Okamura, M., Kodama, K. 1988. The Shimanto belt in Shikoku, Japan - Evolution of Cretaceous to Miocene accretionary prism. Modern Geology 12(1-4), 5-46.

Tanaka, H., Fujimoto, K., Ohtani, T., Ito, H. 2001. Structural and chemical characterization of shear zones in the freshly activated Nojima Fault, Awaji Island, Southwest Japan. Journal of Geophysical Research 106(5), 8789-8810.

Tobin, H., Vannucchi, P., Meschede, M. 2001. Structure, inferred mechanical properties, and implications for fluid transport in the décollement zone, Costa Rica convergent margin. Geology 29(10), 907-910.

Ujiie, K. 2002. Evolution and kinematics of an ancient decollement zone, melange in the Shimanto accretionary complex of Okinawa Island, Ryukyu Arc. Journal of Structural Geology 24(5), 937-952.

Ujiie, K., Hisamitsu, T., Soh, W. 2000. Magnetic and structural fabrics of the melange in the Shimanto accretionary complex, Okinawa Island: Implication for strain history during decollement-related deformation. Journal of Geophysical Research 105(B11), 25729-25742.

Ujiie, K., Hisamitsu, T., Taira, T. 2003. Deformation and fluid pressure variation during initiation and evolution of the plate boundary décollement zone in the Nankai accretionary prism. Journal of Geophysical Research 108(B8), 2398-2411. doi:10.1029/2002JB002314.

Ujiie, K., Maltman, A.J., Sánchez-Gómez, M. 2004. Origin of deformation bands in argillaceous sediments at the toe of the Nankai accretionary prism, southwest Japan. Journal of Structural Geology 26(2), 221-231.

Vannucchi, P., Tobin, H. 2000. Deformation structures and implications for fluid flow at the Costa Rica convergent margin, ODP Sites 1040 and 1043, Leg 170. Journal of Structural Geology 22(8), 1087-1103.

Wallace, R. E., Morris, H.T. 1986. Characteristics of faults and shear zones in deep mines. Pure and Applied Geophysics 124(1-2), 107-125.

Wesnousky, S. G. 2005. The San Andreas and Walker Lane fault systems, western North America: Transpression, transtension, cumulative slip and the structural evolution of a major transform plate boundary. Journal of Structural Geology 27(8), 1505-1512.

Westbrook, G. K., Smith, M.J., Peacock, J.H., Poulter, M.J. 1982. Extensive underthrusting of undeformed sediment beneath the accretionary complex of the Lesser Antilles subduction zone. Nature 300(5893), 625-628.

Wibberley, C. A., Shimamoto, T. 2003. Internal structure and permeability of major strike-slip fault zones: The Median Tectonic Line in Mie Prefecture, Southwest Japan. Journal of Structural Geology 25(1), 59-78.

Wojtal, S. F. 1996. Changes in fault displacement populations correlated to linkage between faults. Journal of Structural Geology 18(2-3), 265-279.

Wong, T., Baud, P., Klein, E. 2001. Localized failure modes in a compactant porous rock. Geophysical Research Letters 28(13), 2521-2524.

VITA

Name:	Takamasa Kanaya
Education:	B.S., Geology, Kochi University, Japan, 2001
	M.S., Geology, Texas A&M University, 2006
Work Experience:	Teaching Assistant, Department of Geology, Texas A&M University, 2003-2006
	Research Technician, Department of Geology, Kochi University, 2001-2002
	Research Assistant, Geological Survey, Japan, 2001
Address:	3 – 12 – 7, Tarumi-ku, Kobe, Hyogo, Japan 655-0044
Email Address:	tkanaya3@hotmail.com